

## Transversely-intersecting D-branes at finite temperature and chiral phase transition

This article has been downloaded from IOPscience. Please scroll down to see the full text article.

JHEP05(2009)035

(<http://iopscience.iop.org/1126-6708/2009/05/035>)

[The Table of Contents](#) and [more related content](#) is available

Download details:

IP Address: 80.92.225.132

The article was downloaded on 03/04/2010 at 09:20

Please note that [terms and conditions apply](#).

# Transversely-intersecting D-branes at finite temperature and chiral phase transition

Mohammad Edalati, Robert G. Leigh and Nam Nguyen Hoang

*Department of Physics, University of Illinois at Urbana-Champaign,  
Urbana IL 61801, U.S.A.*

*E-mail:* [edalati@uiuc.edu](mailto:edalati@uiuc.edu), [rgleigh@uiuc.edu](mailto:rgleigh@uiuc.edu), [nnguyen2@uiuc.edu](mailto:nnguyen2@uiuc.edu)

ABSTRACT: We consider Sakai-Sugimoto like models consisting of  $Dq$ - $Dp$ - $\overline{Dp}$ -branes where  $N_f$  flavor  $Dp$  and  $\overline{Dp}$ -branes transversely intersect  $N_c$  color  $Dq$ -branes along two  $(r + 1)$ -dimensional subspaces. For some values of  $p$  and  $q$ , the theory of intersections dynamically breaks non-Abelian chiral symmetry which is holographically realized as a smooth connection of the flavor branes at some point in the bulk of the geometry created by  $N_c$   $Dq$ -branes. We analyze the system at finite temperature and map out different phases of the theory representing chiral symmetry breaking and restoration. For  $q \leq 4$  we find that, unlike the zero-temperature case, there exist two branches of smoothly-connected solutions for the flavor branes, one getting very close to the horizon of the background and the other staying farther away from it. At low temperatures, the solution which stays farther away from the horizon determines the vacuum. For background D5 and D6-branes we find that the flavor branes, like the zero temperature case, show subtle behavior whose dual gauge theory interpretation is not clear. We conclude with some comments on how chiral phase transition in these models can be seen from their open string tachyon dynamics.

KEYWORDS: Gauge-gravity correspondence, D-branes, Thermal Field Theory

ARXIV EPRINT: [0803.1277](https://arxiv.org/abs/0803.1277)

---

**Contents**

<b>1</b>	<b>Introduction, summary and conclusions</b>	<b>1</b>
<b>2</b>	<b>Transverse intersections at finite temperature</b>	<b>5</b>
2.1	General setup	5
2.2	Flavor $Dp\text{-}\overline{Dp}$ -branes in black D $q$ -brane geometries	7
<b>3</b>	<b>Multiple branches of solutions</b>	<b>9</b>
3.1	Analytical analysis	10
3.2	Numerical analysis for the number of solutions	11
<b>4</b>	<b>Energy of the configurations</b>	<b>14</b>
4.1	Analytical analysis	15
4.2	Numerical results and phase transitions	16
<b>5</b>	<b>Transverse intersections at finite temperature with compact <math>x^q</math></b>	<b>18</b>
5.1	Behavior at high and low temperatures	20
<b>6</b>	<b>Discussion</b>	<b>23</b>
<b>A</b>	<b>Free energies of possible bulk backgrounds</b>	<b>25</b>
A.1	Compact $x^q$	25
A.2	Non-compact $x^q$	33

---

**1 Introduction, summary and conclusions**

A very interesting holographic model of QCD which realizes dynamical breaking of non-Abelian chiral symmetry in a nice geometrical way is the Sakai-Sugimoto model [1]. In this model, one starts with  $N_c$  D4-branes extended in  $(x^0x^1x^2x^3x^4)$ -directions with  $x^4$  being a circle of radius  $R$ . The low energy theory on the branes is a  $(4+1)$ -dimensional  $SU(N_c)$  SYM with sixteen supercharges. To break supersymmetry, anti-periodic boundary condition for fermions around the  $x^4$ -circle must be chosen. To this system,  $N_f$  D8 and  $N_f$   $\overline{D8}$ -branes are added such that they intersect the D4-branes at two  $(3 + 1)$ -dimensional subspaces  $\mathbb{R}^{3,1}$ , and are separated in the compact  $x^4$ -direction by a coordinate distance of  $\ell_0 = \pi R$ . In other words, the D8 and  $\overline{D8}$ -branes are located asymptotically at the antipodal points on the circle. The massless degrees of freedom of the system are the gauge bosons coming from  $4 - 4$  strings and chiral fermions coming from 4-8 strings. (Before compactifying  $x^4$ , there are also massless adjoint scalars and fermions coming from the  $4 - 4$  strings. These modes become massive upon compactifying  $x^4$  and choosing anti-periodic boundary condition for

the adjoint fermions; fermions get masses at tree level whereas scalars get masses due to loop effects.) The fermions localized at the intersection of D4 and D8-branes have (by definition) left-handed chirality and the fermions at the intersection of D4 and  $\overline{\text{D8}}$ -branes are right-handed. The  $U(N_f) \times U(N_f)$  gauge symmetry of the D8 and  $\overline{\text{D8}}$ -branes in this model is interpreted as the chiral symmetry of the fermions living at the intersections. At weak effective four-dimensional 't Hooft coupling  $\lambda_4$  the low energy theory contains QCD but this is not the limit amenable to analysis by the gauge-gravity duality. At strong-coupling ( $\lambda_4 \gg 1$ ), however, the theory is not QCD but can be analyzed using the gauge-gravity duality [2–5], and it has been suggested that it is in the same universality class as QCD. In lack of any rigorous proof for this universality, the best one can do is to check whether this model at large  $N_c$  and large four-dimensional 't Hooft coupling exhibits the key features of QCD; namely, confinement and spontaneous chiral symmetry breaking. In fact, it apparently does [1]. By considering  $N_f$  D8 and  $N_f$   $\overline{\text{D8}}$ -branes as probe “flavor” branes in the near-horizon geometry of  $N_c$  “color” D4-branes and analyzing the Dirac-Born-Infeld (DBI) action of the flavor branes in the background, one observes that at some radial point in the bulk the preferred configuration of the flavor branes is that of smoothly-connected D8 and  $\overline{\text{D8}}$ -branes. This geometrical picture is interpreted as dynamical breaking of  $U(N_f) \times U(N_f)$  chiral symmetry (where the branes are asymptotically separated) down to a single  $U(N_f)$  (where the branes connect). The model also shows confinement [6, 7].

Although choosing  $\ell_0 = \pi R$  makes calculations a bit simpler, there is no particular reason to consider the flavor branes to be asymptotically located at the antipodal points of  $x^4$ . In fact, the  $\ell_0 \ll \pi R$  limit of the Sakai-Sugimoto model is very interesting in its own right. By analyzing the  $\ell_0 \ll \pi R$  limit, or equivalently the  $R \rightarrow \infty$  limit, it was realized in [8] that the theory at the intersections can be analyzed both at weak and strong effective four-dimensional 't Hooft coupling  $\lambda_4$ . At weak-coupling the model can be analyzed using field theoretic methods and in fact is a non-local version of Nambu-Jona-Lasinio (NJL) model [9]. At strong-coupling it can be analyzed by studying the DBI action of the flavor branes in the near-horizon geometry of the color branes and exhibits chiral symmetry breaking via a smooth fusion of the flavor branes at some (radial) point in the bulk. A nice feature of this model is that the scale of chiral symmetry breaking is different from that of confinement [8], and one can completely turn off confinement by taking the  $R \rightarrow \infty$  limit. Therefore the  $\ell_0 \ll \pi R$  limit of the Sakai-Sugimoto model provides a clean holographic model of just chiral symmetry breaking without complications due to confinement.

The finite-temperature analysis (at large  $N_c$  and large 't Hooft coupling  $\lambda_4$ ) of the Sakai-Sugimoto model as well as the holographic NJL model [8], was carried out in [10, 11]. Putting the flavor branes as probes ( $N_f \ll N_c$ ) in the near-horizon geometry of  $N_c$  non-extremal D4-branes and analyzing the DBI action of the flavor branes, one obtains [10, 11] that at low temperatures (compared to  $\ell_0^{-1}$ ) the energetically-favorable solution is that of smoothly-connected D8 and  $\overline{\text{D8}}$ -branes which, like its zero-temperature counterpart, is a realization of chiral symmetry breaking. At high enough temperatures, on the other hand, the preferred (in the path integral sense) configuration is that of disjoint D8 and  $\overline{\text{D8}}$ -branes, hence chiral symmetry is restored. Also, when  $x^4$  is compact and  $\ell_0 < \pi R$ , there exists an intermediate phase where the dual gauge theory is deconfined while chiral symmetry is broken [10].

It is certainly interesting to explore whether the holographic realization of chiral symmetry breaking and restoration is specific to a particular model such as the aforementioned ones, or generic in the sense that other intersecting brane models will realize it, too. To search for genericness (or non-genericness) of chiral symmetry breaking in intersecting brane models, a system of  $Dq$ - $Dp$ - $\overline{Dp}$ -branes was considered at zero temperature in [12] where the color  $Dq$ -branes are stretched in non-compact  $(x^0 x^1 \dots x^q)$ -directions. The flavor  $Dp$  and  $\overline{Dp}$ -branes intersect the color branes at two  $(r + 1)$ -dimensional subspaces  $\mathbb{R}^{r,1}$ . Without flavor branes, the low energy theory on the color branes and whether it can be decoupled from gravity (or other non-field theoretic degrees of freedom) with an appropriate scaling limit was analyzed in [13]. The low energy theory on the  $Dq$ -branes is asymptotically free for  $q < 3$ , conformal for  $q = 3$ , and infrared free for  $q > 3$ . While for  $q \leq 5$ , there always exists a scaling limit for which the open string modes can be decoupled from the closed string modes, there exists no such limit for  $q = 6$ . With the flavor branes present, an analysis was carried out in [12] where the behavior of the model for both small and large effective 't Hooft coupling  $\lambda_{\text{eff}} \sim \lambda_{q+1} \ell_0^{3-q}$  ( $\ell_0$  is the asymptotic coordinate distance between  $Dp$  and  $\overline{Dp}$ -branes, and  $\lambda_{q+1}$  is the 't Hooft coupling of the  $(q+1)$ -dimensional theory on the  $Dq$ -branes.) was considered. Taking the  $N_c \rightarrow \infty$  limit while keeping  $\lambda_{\text{eff}}$  fixed and large, amounts, in the probe approximation, to putting the flavor branes in the near-horizon geometry of  $N_c$  color branes. (See [12, 13] for the validity of the supergravity analysis in these models.) Determining the shape of the flavor branes (relevant for chiral symmetry breaking) by analyzing their DBI action in the background geometry, it was observed that [12] for  $q \leq 4$  there always exists a smoothly-connected brane solution which is energetically favorable. For a subclass of these general intersecting brane models, namely those for which  $q + p - r = 9$ , the above-mentioned connected solutions can be identified with the  $U(N_f) \times U(N_f)$  chiral symmetry being spontaneously broken. Following [12] we will call the brane models for which  $q + p - r = 9$  as transversely-intersecting brane models and their intersections as transverse intersections. For  $q = 5$ , there exists no connected solution except when  $\ell_0$  takes a particular value. For this particular value of  $\ell_0$  which is around the scale of non-locality of the low energy theory on the D5-branes (which is a little string theory; see [14] for a review of little string theories), there is a continuum of connected solutions whose turning points can be anywhere in the radial coordinate of the bulk geometry. All such solutions are equally energetically favorable. For  $q = 6$ , there is a connected solution but is not the preferred one. The more energetically favorable solution, in this case, is that of disjoint branes. Due to the lacking of an appropriate decoupling limit for  $q = 6$ , it is not clear whether one can realize such a solution as a phase for which chiral symmetry is unbroken.

**Summary and conclusions.** The purpose of this paper is to investigate some aspects of non-compact transversely-intersecting D-brane models at finite temperature, in particular the number of solutions, their behavior, and whether or not such solutions can be identified with a chirally broken (or restored) phase of the dual gauge theory living at the intersections. The main reason for us to consider transverse intersections is that in the probe approximation the generalization of the Abelian  $U(1) \times U(1)$  chiral symmetry to the non-Abelian case is straightforward: one just replaces  $N_f = 1$  with general  $N_f$ , and multiplies

the flavor DBI action by  $N_f$ . This is *not* the case in other holographic models of chiral symmetry breaking and restoration.<sup>1</sup> Note that the Sakai-Sugimoto model [1], its non-compact version [8], and the D2-D8- $\overline{\text{D8}}$  model analyzed in [17] which holographically realizes a non-local version of the Gross-Neveu model [18] are examples of transverse intersections.

This paper is organized as follows. In section two we first review the general set up of the transversely-intersecting  $Dq\text{-}Dp\text{-}\overline{Dp}$ -branes, then consider the system at finite temperature at large  $N_c$  and large effective 't Hooft coupling  $\lambda_{\text{eff}}$ . There are two saddle point contributions (thermal and black brane) to the bulk Euclidean path integral, and each can potentially be used as a background geometry dual to the color theory. Comparing the free energies of the two saddle points, we determine which one is dominant (has lower free energy) for various  $q$ 's. For  $q \neq 5$ , the dominant saddle point is the black brane geometry, whereas for  $q = 5$ , the thermal geometry is typically dominant. In section three we present the solutions to the equation of motion for the DBI action of the flavor branes placed in the near horizon geometry of black  $Dq$ -branes. By a combination of analytical and numerical techniques, we show that, unlike the zero-temperature case, for  $\ell_0/\beta$  less than a critical value, there exist generically two branches of smoothly-connected solutions (and of course, a solution with disjoint branes) for  $q \leq 4$ . ( $\beta$  is the circumference of the asymptotic Euclidean time circle, and is equal to the inverse of the dual gauge theory temperature  $T$ .) Note that some of these branches were previously missed in the literature. One branch which we will call the “long” connected solution gets very close to the horizon of the black  $Dq$ -branes whereas the other one named “short” connected solution stays farther away from it. Beyond the critical value, the flavor branes are “screened” and cannot exist as a connected solution. The situation is, however, different for  $q = 5, 6$ . For  $q = 5$  and  $T < (2\pi R_{5+1})^{-1}$ , where  $R_{5+1}$  denotes the characteristic radius of the D5-brane geometry, the flavor branes must be placed in the near horizon geometry of thermal D5-branes. Like the zero temperature case, we find that there exists an infinite number of connected solutions when  $\ell_0$  is around the non-locality scale of the low energy theory on the D5-branes. This scale is set by the (inverse) hagedorn temperature of D5-brane little string theory. There are no connected solution for other values of  $\ell_0$ , though. For  $T = (2\pi R_{5+1})^{-1}$  the flavor branes should be considered in the near horizon geometry of black D5-branes. In this case there always exists one connected solution, as well as a disjoint solution, for small  $\ell_0$  (compared to  $(2\pi R_{5+1})^{-1}$ ). In fact, at this particular temperature there is one connected solution for  $\ell_0$ 's much less than  $R_{5+1}$ . The number of solutions for  $\ell_0$  beyond the non-locality scale ( $\sim R_{5+1}$ ) depends on the dimension of the intersections. For four-dimensional intersections, there are two connected solutions up to a critical value whereas for two-dimensional intersections there is no connected solution. Of course, for both two- and four-dimensional intersection there is always a solution representing disjoint branes. Having determined the flavor brane solutions in the background of thermal and black D5-branes, it is not clear whether or how these solutions represent a chirally-broken or restored phase in the dual theory, mainly because in the geometry of D5 – branes, there are modes (non-field theoretic) which cannot totally be

---

<sup>1</sup>For non-transverse intersections, namely  $q + p - r \neq 9$ , one can identify a symmetry in the common transverse direction as a chiral symmetry for the fermions of the intersections [15]. In some cases the generalization to low-rank non-Abelian chiral symmetry is possible [16], but such generalizations are not generic.

decoupled from the dual field theory degrees of freedom. Lastly, for  $q = 6$ , independent of what value  $\ell_0/\beta$  takes, there always exist one connected solution (and a disjoint solution).

In section four, we map out different phases of the dual gauge theories and determine whether or not there is a chiral symmetry breaking-restoration phase transition. We do this by comparing the regularized free energies of the various branches of the solutions found in section three. For  $q \leq 4$  the short solution is preferred to both long and disjoint solutions at small enough temperatures (compared to  $\ell_0^{-1}$ ), hence chiral symmetry is broken. At high temperatures, however, chiral symmetry gets restored and this phase transition is first order. For  $q = 5$  and  $T < (2\pi R_{5+1})^{-1}$ , the infinite number of connected solutions are all equally energetically favorable, and each one of them is preferred over the disjoint solution. For  $T = (2\pi R_{5+1})^{-1}$ , we find that for small enough  $\ell_0/(2\pi R_{5+1})$  the disjoint solution is preferred. For larger values of  $\ell_0$ , there is no connected solution so the disjoint solution is the vacuum. As we alluded to earlier, it is not clear to us that the preferred solutions of the flavor branes in the background of color D5-branes can be associated with different phases of the dual theory. For  $q = 6$ , although we find that the disjoint solution is always preferred and there is no phase transition, there is no clear way to associate this solution with unbroken chiral symmetry in the dual field theory. This is because there is no decoupling limit that one can take to separate the gravitational degrees of freedom of those of the dual theory.

Section five is devoted to a brief analysis of the number of solutions and their energies for transversely-intersecting  $Dq$ - $Dp$ - $\overline{Dp}$ -branes with compact  $x^q$ . In section six we speculate how the order parameter for chiral symmetry breaking can be realized in finite-temperature transversely-intersecting D-branes by including the thermal dynamics of an open string tachyon stretched between the flavor branes, and how it may depend on temperature. Finally, in the appendix we present detailed calculations for the free energies of the near horizon geometries of color  $Dq$ -branes (with the topology of either  $S^1 \times S^1$  or  $S^1 \times \mathbb{R}$  in the  $t - x^q$  submanifold) to determine the dominant background geometry (either thermal or black brane) at low and high temperatures.

## 2 Transverse intersections at finite temperature

We start this section by reviewing first the general setup for transverse intersections of  $Dq$ - $Dp$ - $\overline{Dp}$ -branes and identifying the massless degrees of freedom at intersections. We consider the system at finite temperature in the large  $N_c$  and large 't Hooft coupling limits. Since there is more than one background, we determine the one with the lowest free energy and consider that as the background dual to the color sector of the dual theory at finite temperature. We then write the equation of motion for the flavor branes. This section is followed in the next section by an analysis of the solutions to the equation of motion as a function of the dimensions of the intersections  $r$ , as well as  $q$ . (For transverse intersections  $p$ , the spacial dimension of the flavor branes, is determined once  $r$  and  $q$  are given.)

### 2.1 General setup

Consider a system of intersecting  $Dq$ - $Dp$ - $\overline{Dp}$ -branes in flat non-compact ten-dimensional Minkowski space where  $N_c$   $Dq$ -branes are stretched in  $(x^0 x^1 \dots x^q)$ -directions, and each

stack of  $N_f$   $Dp$  and  $N_f$   $\overline{Dp}$ -branes are extended in  $(x^0 x^1 \dots x^r)$ - and  $(x^{q+1} \dots x^9)$ -directions. The  $Dp$ - and  $\overline{Dp}$ -branes are separated in the  $x^q$ -direction by a coordinate distance  $\ell_0$  and intersect the  $Dq$ -branes at two  $(r+1)$ -dimensional intersections

$$\begin{array}{cccccccc}
 & x^0 & x^1 & \dots & x^r & \dots & x^q & \dots & x^9 \\
 Dq & \times & \times & \dots & \times & \dots & \times & \dots & \cdot \\
 Dp & \times & \times & \dots & \times & \dots & \cdot & \dots & \times \\
 \overline{Dp} & \times & \times & \dots & \times & \dots & \cdot & \dots & \times.
 \end{array} \tag{2.1}$$

Using T-duality one can determine the massless degrees of freedom localized at the intersection. It turns out that for transverse intersections,  $q+p-r=9$ , the massless modes which come from the Ramond sector in the  $p-q$  strings are Weyl fermions. These fermions are in the fundamentals of  $U(N_c)$  and  $U(N_f)$ . The massless modes at the other intersection are also Weyl fermions which transform in the fundamentals of  $U(N_c)$  and  $U(N_f)$  of the  $\overline{Dp}$ -branes.

One way to put the above system at finite temperature (at large  $N_c$ , large effective 't Hooft coupling  $\lambda_{\text{eff}}$ , and in the probe approximation  $N_f \ll N_c$ ) is to start with the geometry of black  $Dq$ -branes as background. The Euclidean metric for this geometry is

$$ds^2 = \left( \frac{u}{R_{q+1}} \right)^{\frac{7-q}{2}} \left( f(u) dt^2 + d\vec{x}^2 \right) + \left( \frac{u}{R_{q+1}} \right)^{-\frac{7-q}{2}} \left( \frac{du^2}{f(u)} + u^2 d\Omega_{8-q}^2 \right), \tag{2.2}$$

with

$$f(u) = 1 - \left( \frac{u_T}{u} \right)^{7-q}, \tag{2.3}$$

where in the metric  $d\Omega_{8-q}^2$  is the line element of a  $(8-q)$ -sphere with a radius equal to unity, and  $R_{q+1}$ , which denotes the characteristic radius of the geometry, is given by

$$R_{q+1}^{7-q} = (2\sqrt{\pi})^{5-q} \Gamma\left(\frac{7-q}{2}\right) g_s N_c l_s^{7-q} = 2^{7-2q} (\sqrt{\pi})^{9-3q} \Gamma\left(\frac{7-q}{2}\right) g_{q+1}^2 N_c l_s^{10-2q}, \tag{2.4}$$

where  $g_s$  is the string coupling. The Euclidean time is periodically identified:  $t \sim t + \beta$ , where  $\beta$  is equal to the inverse of the temperature  $T$  of the black branes. In (2.3) the horizon radius  $u_T$  is related to  $\beta$  as

$$T = \beta^{-1} = \frac{7-q}{4\pi} \left( \frac{u_T}{R_{q+1}} \right)^{\frac{7-q}{2}} \frac{1}{u_T}. \tag{2.5}$$

The relationship between  $u_T$  and  $\beta$  comes about in order to avoid a conical singularity in the metric at  $u = u_T$ . Note that for black D5-branes  $\beta$  is independent of  $u_T$ , and equals  $2\pi R_{5+1}$ .

Also, the dilaton  $\phi$  and the  $q$ -form RR-flux  $F_q$  are given by

$$e^\phi = g_s \left( \frac{u}{R_{q+1}} \right)^{\frac{1}{4}(q-3)(7-q)}, \quad F_q = \frac{2\pi N_c}{V_{8-q}} \epsilon_{8-q}, \tag{2.6}$$

where  $V_{8-q}$  and  $\epsilon_{8-q}$  are the volume and the volume form of the unit  $(8-q)$ -sphere, respectively.



There is, however, another background with the same asymptotics as (2.2) which may potentially compete with the aforementioned background. The metric for this (thermal) geometry is

$$ds^2 = \left(\frac{u}{R_{q+1}}\right)^{\frac{7-q}{2}} (dt^2 + d\vec{x}^2) + \left(\frac{u}{R_{q+1}}\right)^{-\frac{7-q}{2}} (du^2 + u^2 d\Omega_{8-q}^2), \quad (2.7)$$

with the Euclidean time  $t$  being periodically identified with a period  $\beta = T^{-1}$ . Unlike the black brane geometries (2.2),  $\beta$  could take arbitrary values in the thermal geometries (2.7). The dilaton and the  $q$ -form RR-flux are the same as (2.6).

In the appendix we have calculated the free energies of both thermal and black brane geometries. Except for  $q = 5$ , the difference in free energies  $\Delta S$  of the two geometries subject to the same asymptotics is given by

$$\Delta S = S_{\text{thermal}} - S_{\text{black brane}} = \frac{9-q}{g_s^2} V_9 u_T^{7-q}, \quad (2.8)$$

where  $V_9$  is the volume of space transverse to the radial coordinate  $u$ :  $V_9 = \text{Vol}(S^{8-q})\text{Vol}(\mathbb{R}^q)\text{Vol}(S^1_\beta)$ . The volume  $V_9$  is measured in string unit  $l_s$  where for simplicity we set  $l_s = 1$ . The difference in free energies (2.8) shows that the thermal background is less energetically favorable compared to the black brane background (2.2). Thus, there is no Hawking-Page type transition between the two geometries which holographically indicates that there is no confinement-deconfinement phase transition in the dual theory. The situation is different for  $q = 5$ . Semi-classically, once the characteristic radius  $R_{5+1}$  is given, the black D5-brane geometry will have a fixed temperature  $T = (2\pi R_{5+1})^{-1}$ . At this specific temperature, there are two saddle points contributing to the (type IIB) supergravity path integral: thermal and black D5-brane geometries. The difference in free energies of the two saddle points is (see the appendix for more details)

$$S_{\text{thermal D5}} - S_{\text{black D5-brane}} = \frac{8\pi}{g_s^2} \text{Vol}(S^3)\text{Vol}(\mathbb{R}^5)R_{5+1}u_T^2, \quad \text{at } \beta = 2\pi R_{5+1}, \quad (2.9)$$

showing that the black brane geometry is the saddle point with lower free energy. However, at temperatures other than  $(2\pi R_{5+1})^{-1}$ , the thermal geometry is the only saddle point, although due to the hagedorn temperature of the D5-brane theory, one should only consider temperatures less than  $(2\pi R_{5+1})^{-1}$ . Thus, for  $T < (2\pi R_{5+1})^{-1}$  we use the thermal D5-brane geometry as background.

## 2.2 Flavor $Dp$ - $\overline{Dp}$ -branes in black $Dq$ -brane geometries

We are interested in the dynamics of the flavor  $Dp$  and  $\overline{Dp}$ -branes in the background of the black  $Dq$ -brane geometries. As we alluded to earlier, for  $q = 5$  the thermal geometry of  $N_c$  D5-branes (once the limit of the near horizon geometry is taken) is the background that one should use for the dual finite temperature field theory for  $T < (2\pi R_{5+1})^{-1}$ . We also analyze the dynamics of the flavor branes in the background of the black D5-branes in which case it is understood that the dual theory is at a fixed temperature  $T = (2\pi R_{5+1})^{-1}$ . We are

interested in the static shape of the flavor branes as a function of the radial coordinate  $u$ . Therefore we choose the embedding

$$\begin{aligned} t = \sigma^0, & & x^1 = \sigma^1, & & \dots & & x^r = \sigma^r, & & x^q = \sigma^q, \\ u = u(\sigma^q), & & x^{q+2} = \sigma^{q+1}, & & \dots & & x^8 = \sigma^{p-1}, & & x^9 = \sigma^p, \end{aligned} \quad (2.10)$$

subject to the boundary condition

$$u\left(\pm\frac{\ell_0}{2}\right) = \infty, \quad (2.11)$$

where  $\{\sigma^0, \dots, \sigma^p\}$  are the worldvolume coordinates of the flavor branes. This boundary condition simply states that the asymptotic coordinate distance between the  $Dp$  and  $\overline{Dp}$ -branes is  $\ell_0$ . Ultimately the stability of such an assumption lies in the large  $N_c$  limit.

From now on, we set  $N_f = 1$ . As it becomes apparent in what follows, the generalization to  $N_f \ll N_c$  is straightforward. The dynamics of a  $Dp$ -brane (and a  $\overline{Dp}$ -brane) is determined by its DBI plus Chern-Simons action. Solving the equations of motion for the gauge field, one can safely set the gauge field equal to zero and just work with the DBI part of the action. After all, it is this part of the full action which is relevant for our purpose of determining the shape of the  $Dp$  and  $\overline{Dp}$ -branes. Therefore, with gauge field(s) set equal to zero, the dynamics is captured by the DBI action

$$S_{\text{DBI}} = \mu_p \int d^{p+1}\sigma e^{-\phi} \sqrt{\det(g_{ab})}, \quad (2.12)$$

where  $\mu_p$  is a constant, and  $g_{ab} = G_{MN} \partial_a x^M \partial_b x^N$  is the induced metric on the worldvolume of the  $Dp$ -brane. For a  $Dp$ -brane forming a curve  $u = u(x^q)$ , the DBI action (2.12) reads

$$S_{\text{DBI}} = \beta C(q, r) \int dx^q u^{\frac{\gamma}{2}} \left[ f(u) + \left( \frac{u}{R_{q+1}} \right)^{2\delta} u'^2 \right]^{\frac{1}{2}}, \quad (2.13)$$

where

$$\begin{aligned} C(q, r) &= \frac{\mu_p}{g_s} \text{Vol}(S^{8-q}) R_{q+1}^{\frac{1}{4}(q-7)(r-3)}, \\ \gamma &= 2 + \frac{1}{2}(7-q)(r+1), \\ \delta &= \frac{1}{2}(q-7), \end{aligned} \quad (2.14)$$

and  $u' = du/dx^q$ . For a  $Dp$ -brane forming a curve  $u(x^q)$  in the thermal D5-brane geometry the DBI action is obtained by setting  $f(u) = 1$  in (2.13). The integrand in (2.13) does not explicitly depend on  $x^q$ , therefore  $\mathcal{L} - u' \partial \mathcal{L} / \partial u'$  must be conserved (with respect to  $x^q$ ). A first integral of the equation of motion is then obtained

$$u^{\frac{\gamma}{2}} f(u) \left[ f(u) + \left( \frac{u}{R_{q+1}} \right)^{2\delta} u'^2 \right]^{-\frac{1}{2}} = u_0^{\frac{\gamma}{2}}, \quad (2.15)$$

where  $u_0$  parametrizes the solutions. We now analyze the solutions of (2.15).

### 3 Multiple branches of solutions

The simplest solution of the equation of motion in (2.15), namely  $u_0 = 0$ , corresponds to  $x^q = \text{constant}$ . In order to satisfy the boundary condition (2.11), one obtains  $x^q = \pm \ell_0/2$ . So, the  $u_0 = 0$  solution corresponds to disjoint Dp and  $\overline{\text{Dp}}$ -branes descending all the way down to the horizon at  $u = u_T$ . Also, note that the existence of this solution is independent of  $\beta$ .

For  $u_0 \neq 0$ , solving for  $u'$  yields

$$u'^2 = \frac{1}{u_0^\gamma} \left( \frac{u}{R_{q+1}} \right)^{-2\delta} f(u) \left( u^\gamma f(u) - u_0^\gamma \right). \quad (3.1)$$

Since the left hand side of (3.1) is non-negative, the right hand side of (3.1) must also be non-negative resulting in  $u \geq \max\{u_T, u_*\}$ , where  $u_*$  is a possible turning point. Therefore, for allowed solutions one must have  $u \geq u_* > u_T$ .

The possible turning points are determined by analyzing the zeros of the right hand side of (3.1). Setting  $f(u_*) = 0$  will not result in a valid turning point. So, the other possibilities come from solving  $u_*^\gamma f(u_*) - u_0^\gamma = 0$ , which we will rewrite as follows

$$u_*^\gamma - u_*^\sigma u_T^{-2\delta} - u_0^\gamma = 0, \quad (3.2)$$

where

$$\sigma = \gamma + 2\delta = 2 + \frac{1}{2}(7 - q)(r - 1). \quad (3.3)$$

Note that since  $r \neq 0$  (and in fact, for the cases of interest, it is either 1 or 3),  $\sigma$  is always a positive integer which, combined with the fact that  $\delta < 0$ , implies that  $\sigma < \gamma$ .

We use (3.1) to relate the integration constant  $u_*$ , or equivalently  $u_0$ , to the parameters of the theory, namely the (inverse) temperature  $\beta$  and the asymptotic distance between the Dp and  $\overline{\text{Dp}}$ -branes  $\ell_0$ . First, rearrange (3.1) to get

$$\begin{aligned} x^q(u) &= R^{-\delta} u_0^{\frac{\gamma}{2}} \int_{u_*}^u \left( u^{-2\delta} - u_T^{-2\delta} \right)^{-\frac{1}{2}} \left( u^\gamma - u^\sigma u_T^{-2\delta} - u_0^\gamma \right)^{-\frac{1}{2}} du \\ &= R^{-\delta} (u_*^\gamma - u_*^\sigma u_T^{-2\delta})^{\frac{1}{2}} \int_{u_*}^u \left( u^{-2\delta} - u_T^{-2\delta} \right)^{-\frac{1}{2}} \left( u^\gamma - u^\sigma u_T^{-2\delta} - (u_*^\gamma - u_*^\sigma u_T^{-2\delta}) \right)^{-\frac{1}{2}} du, \end{aligned} \quad (3.4)$$

where in the second line we used (3.2) to trade  $u_0$  for  $u_*$ . Changing to a new (dimensionless) variable  $z = u/u_T$ , (3.4) becomes

$$x^q(z) = -\frac{\delta}{2\pi} \beta (z_*^\gamma - z_*^\sigma)^{\frac{1}{2}} \int_{z_*}^z \left( \tilde{z}^{-2\delta} - 1 \right)^{-\frac{1}{2}} \left( \tilde{z}^\gamma - \tilde{z}^\sigma - (z_*^\gamma - z_*^\sigma) \right)^{-\frac{1}{2}} d\tilde{z}, \quad (3.5)$$

where  $z_* \in (1, \infty)$ . Taking the  $z \rightarrow \infty$  limit, we can relate  $z_*$  to  $\beta$  and  $\ell_0$

$$\frac{\ell_0}{\beta} = -\frac{\delta}{\pi} (z_*^\gamma - z_*^\sigma)^{\frac{1}{2}} \int_{z_*}^{\infty} \left( z^{-2\delta} - 1 \right)^{-\frac{1}{2}} \left( z^\gamma - z^\sigma - (z_*^\gamma - z_*^\sigma) \right)^{-\frac{1}{2}} dz. \quad (3.6)$$

As we mentioned earlier, the solutions to the equation of motion are parametrized by possible value(s) of the turning point  $z_*$ . For a fixed  $\ell_0/\beta$ , it is the number of  $z_*$  which determines the number of (connected) solutions. Thus, one has to analyze  $\ell_0/\beta$  as a function of  $z_*$  to determine the number of solutions for a fixed  $\ell_0/\beta$ .

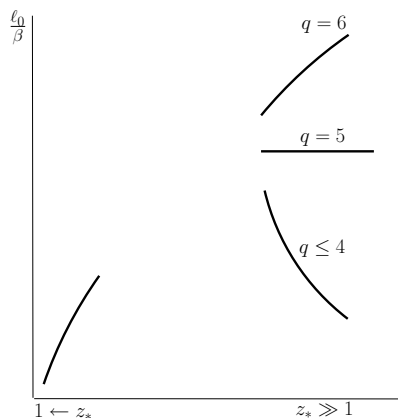


**Figure 1.** Behavior of  $\ell_0/\beta$  versus  $z_*$  in two regions of  $z_* \rightarrow 1$  and  $z_* \gg 1$  for various  $q$ 's. Except for  $q = 5$ , these plots illustrate the number of connected  $Dp$ -branes at low and high temperatures placed in the background of black  $Dq$ -branes. For  $q = 5$ , it is understood that  $\beta$  is fixed;  $\beta = 2\pi R_{5+1}$ , and different solutions is obtained by varying  $\ell_0$ .

### 3.1 Analytical analysis

There are regions of  $z_*$  for which  $\ell_0/\beta$  as a function of  $z_*$  can be given analytically. These are the  $z_* \rightarrow 1^+$  and  $z_* \gg 1$  regions. For any  $z_*$ , the integral in (3.6) can be evaluated numerically. The numerical results will be presented shortly after the analytical analysis for the two limiting cases is given.

First consider the  $z_* \rightarrow 1^+$  limit. Taking  $z_* = 1 + \epsilon$  where  $0 < \epsilon \ll 1$ , (3.6) is approximated by

$$\frac{\ell_0}{\beta} \sim -\frac{\delta}{\pi} \sqrt{-2\delta\epsilon} \int_{1+\epsilon}^{\infty} (z^{-2\delta} - 1)^{-\frac{1}{2}} (z^\gamma - z^\sigma + 2\delta\epsilon)^{-\frac{1}{2}} dz. \tag{3.7}$$

Ignoring some numerical prefactors, the behavior of (3.7), is approximated by  $\sqrt{\epsilon} \int_{1+\epsilon}^{\infty} z^{\delta-\frac{\gamma}{2}} dz$  for large values of  $z$ . Since  $\delta - \frac{\gamma}{2} < -2$  for all  $q$  and  $r$  of interest, one has  $\sqrt{\epsilon} \int_{1+\epsilon}^{\infty} z^{\delta-\frac{\gamma}{2}} dz \sim \sqrt{\epsilon}$ . On the other hand, when  $z$  approaches  $z_*$  such that  $z - z_* > 0$ , we define  $z = z_* + x$  with  $0 < x \ll 1$ , and expand out the integrand of (3.7) around  $x$ . We get

$$\begin{aligned} \frac{\ell_0}{\beta} &\sim -\frac{\delta}{\pi \sqrt{-2\delta}} \sqrt{\epsilon} \int_0^{\infty} (x(x+\epsilon))^{-\frac{1}{2}} dx \\ &\sim -\frac{1}{\pi} \sqrt{-2\delta} \sqrt{\epsilon} \log \sqrt{\epsilon}, \end{aligned} \tag{3.8}$$

indicating that the leading behavior of  $\ell_0/\beta$  in the  $z_* \rightarrow 1$  limit is  $-\sqrt{\epsilon} \log \sqrt{\epsilon}$ .

For the  $z_* \gg 1$  region, we can approximate (3.6) by (recall  $\delta < 0$  and  $\sigma < \gamma$ )

$$\begin{aligned} \frac{\ell_0}{\beta} &\sim -\frac{\delta}{\pi} z_*^{\frac{\gamma}{2}} \int_{z_*}^{\infty} z^\delta (z^\gamma - z_*^\gamma)^{-\frac{1}{2}} dz + \dots \\ &= -\frac{\delta}{\pi} z_*^{1+\delta} \int_1^{\infty} y^\delta (y^\gamma - 1)^{-\frac{1}{2}} dy + \dots \\ &= -\frac{\delta}{\gamma \sqrt{\pi}} \frac{\Gamma\left[\frac{\gamma-2(1+\delta)}{2\gamma}\right]}{\Gamma\left[\frac{\gamma-(1+\delta)}{\gamma}\right]} z_*^{1+\delta} + \dots, \end{aligned} \tag{3.9}$$

where  $\dots$  represents terms subleading in  $z_*$ , and in the second line in (3.9) we have changed the variable from  $z$  to  $y = z/z_*$ . Thus, aside from a numerical factor, the  $z_* \rightarrow \infty$  limit of (3.6) reads

$$\frac{\ell_0}{\beta} \sim z_*^{1+\delta}. \tag{3.10}$$

This expression is identical to the one derived for the zero temperature case in [12]. This resemblance is not accidental because the large  $z_*$  limit corresponds to having a turning point very far away from the horizon of the background geometry. The results obtained for this limit should then match those derived for the zero temperature case. An interesting feature of (3.10) is that for the black D5-branes  $\ell_0/(2\pi R_{5+1})$  is independent of  $z_*$  and approaches a constant value of  $1/(r+3)$ . This value has been argued in [12] to be around the scale of non-locality of the low energy effective theory on D5-branes. The analysis for the dynamics of the flavor branes placed in the thermal D5-brane geometry is the same as the analysis when they are placed in the zero temperature D5-brane geometry. The zero temperature analysis has already been done in [12] where it was found that there exist an infinite number of connected solutions for one specific value of  $\ell_0 = 2\pi R_{5+1}/(r+1)$ , and none for other  $\ell_0$ 's.

Analyzing (3.6) for the two regions of  $z_* \rightarrow 1^+$  and  $z_* \gg 1$ , the minimum crude conclusion that one can draw is that for small enough  $\ell_0/\beta$  there exist two connected solutions (one closer to the horizon which we will name "long" connected solution, and the other farther away from it named "short" connected solution) for  $q \leq 4$  and only one curved solution for  $q = 6$ . For  $q = 5$  and for  $T < (2\pi R_{5+1})^{-1}$ , there exists an infinite number of connected solutions for just  $\ell_0 = 2\pi R_{5+1}/(r+1)$  and none for others. On the other hand, for  $T = (2\pi R_{5+1})^{-1}$ , there is only one connected solution given that  $\ell_0 \ll 2\pi R_{5+1}$ . The analysis for the two  $z_*$  regions has been summarized in figure 1.

### 3.2 Numerical analysis for the number of solutions

For generic values of  $\ell_0/\beta$ , the allowed number of solutions can be determined by numerically integrating (3.6) and plotting  $\ell_0/\beta$  versus  $z_*$ . The results for various intersections and Dq-branes are shown in figure 2. Although we have plotted  $\ell_0/\beta$  versus  $z_*$  for  $z_* \in (1, 50)$ , the qualitative behavior of the plots stays the same if one considered larger values of  $z_*$ . As we will describe below, the number of curved solutions depends on what configuration is being considered. Note that regardless of the configuration, there always exists a disjoint solution. In what follows in the rest of this subsection, when we say there exist one or two solutions for a particular system we have connected solutions in mind.

**(3 + 1)-dimensional intersections.** In this case there are three allowed D-brane configurations which are transversely intersecting. These are the D4-D8- $\bar{D}8$ , D5-D7- $\bar{D}7$  and D6-D6- $\bar{D}6$  configurations shown on the top row in figure 2.

For the D4-D8- $\bar{D}8$  configuration (shown on the upper left corner in figure 2), there is a critical value of  $(\ell_0/\beta)_{cr} \approx 0.17$  beyond which there exists no connected solution for the flavor branes. Below this critical value there are two connected solutions which we earlier called the "short" and the "long" connected solutions. The existence of these two types

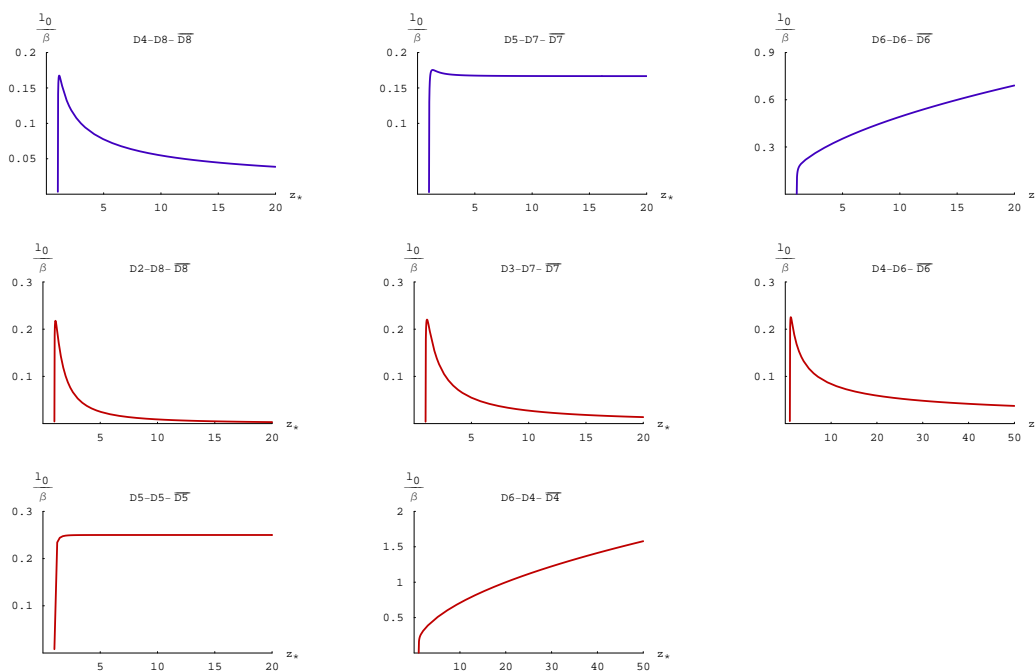


**Figure 2.** Behavior of  $\ell_0/\beta$  versus  $z_*$  obtained numerically for generic values  $z_*$  for various  $q$ 's and intersections of interest, i.e.  $r = 1$  and  $r = 3$ . The blue plots show the behavior for  $3 + 1$  intersections whereas the red plots show the behavior for  $1 + 1$  intersections. These plots show the number of connected  $Dp$ -branes (for all temperatures) placed in the background of black  $Dq$ -branes. For  $q = 5$ , the temperature  $T$  is fixed:  $T = (2\pi R_{5+1})^{-1}$ . Except for  $q = 5, 6$ , such solutions can potentially be realized as different phases of the holographic dual theories.

of solutions and the critical value of 0.17 were already noted by the authors of [11] in the their analysis of the holographic NJL model at finite temperature. We will see in the next section that the short solution is always more energetically favorable to the long one. Since there also exists a disjoint solution, determining the chirally-broken or chirally-symmetric phase of the dual field theory (which is a non-local version of the NJL model [8]) is just a matter of comparing the free energies of the disjoint and short connected solution. This will be done in the next section.

The analysis for the  $D5-D7-\bar{D}7$  and  $D6-D6-\bar{D}6$  cases are, however, more subtle, and the holographic interpretation of the solutions is less transparent for reasons to be mentioned below. For the  $D5-D7-\bar{D}7$  configuration at temperature  $T = (2\pi R_{5+1})^{-1}$ , there are two critical values of  $(\ell_0/(2\pi R_{5+1}))_{cr} \approx 0.168$  and  $0.175$ . For  $\ell_0/(2\pi R_{5+1}) < 0.168$  there is always one connected solution, for  $0.168 < \ell_0/(2\pi R_{5+1}) < 0.175$  there are two, and for  $\ell_0/(2\pi R_{5+1}) > 0.175$  there exists none. Comparing these results to the ones obtained for the zero-temperature  $D5-D7-\bar{D}7$  configuration, one observes that while at zero temperature [12], there are either an infinite number of solutions or none, at  $T = (2\pi R_{5+1})^{-1}$  there are different numbers of solutions (one, two, or none) depending on what values  $\ell_0$  take; see figures 2 and 3. For  $D5-D7-\bar{D}7$  configuration at temperatures

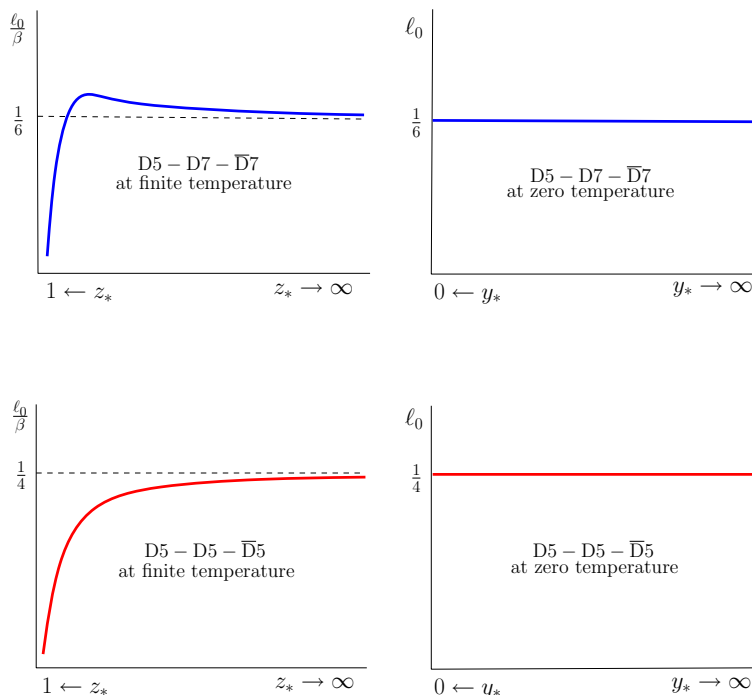


**Figure 3.** The two plots on the left hand side show the number of connected solutions for the flavor D7 and D5-branes in the background of black D5-branes at  $T = (2\pi R_{5+1})^{-1}$ . The plots on the right hand side, on the other hand, show the number of connected solutions for the same flavor branes in the background of thermal (or zero temperature) D5-branes.  $z_*$ 's represent the turning points of the connected flavor branes in the black D5-brane geometry while  $y_*$ 's are the turning points in the background of thermal D5-branes.

$T < (2\pi R_{5+1})^{-1}$ , the situation is the same as the zero temperature case. There exist connected solutions only for a specific value of  $\ell_0 = \pi R_{5+1}/3$ . Indeed, there are an infinite number of such solutions; see figure 3.

For D6-D6-D6-bar configuration, the situation is simpler. For any  $\ell_0/\beta$  there always exists one and only one connected solution. As we will see in the next section all these connected solutions are less energetically favorable compared to disjoint solutions. The observation that for color D6-branes at finite temperature there is always one connected solution, hence no "screening length", is in accord with the fact that the near horizon geometry of D6-branes cannot be decoupled from the gravitational modes of the bulk geometry [13].

**(1 + 1)-dimensional intersections.** In this case, there are five allowed configurations (shown on the second and third rows in figure 2), namely D2-D8-D8-bar, D3-D7-D7-bar, D4-D6-D6-bar, D5-D5-D5-bar and D6-D4-D4-bar. Configurations with  $q \leq 4$  show similar behavior. For  $q \leq 4$  there always exists a critical  $(\ell_0/\beta)_{cr}$  beyond which connected solutions cease to exist. The critical value obtained from figure 2 is  $(\ell_0/\beta)_{cr} \approx 0.225, 0.223, 0.227$  for color D2, D3 and D4-branes, respectively. Below these critical values there are two solutions, the short and long solutions.<sup>2</sup>

<sup>2</sup>The authors of [17] studied the D2-D8-D8-bar system at finite temperature but missed the existence of the long connected solution.

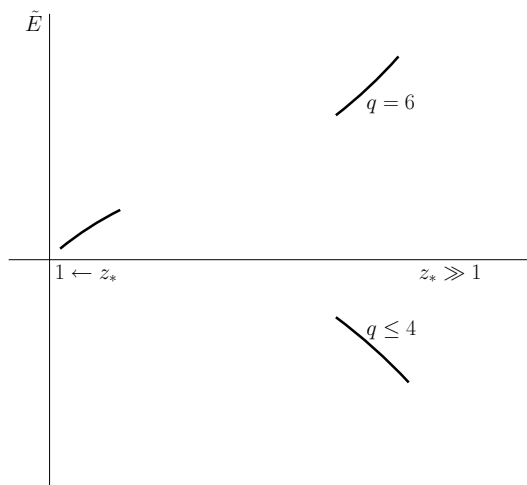


**Figure 4.** Behavior of  $\tilde{E}$  versus  $z_*$  obtained numerically for generic values of  $z_*$  for various  $q$ 's.

For the D5-D5- $\bar{D}5$  system at  $T = (2\pi R_{5+1})^{-1}$ , below a critical value of  $(\ell_0/(2\pi R_{5+1}))_{\text{cr}} \approx 0.251$  there is always one solution whereas above this value connected solutions do not exist. Note the difference (depicted in figure 3) of this case with the D5-D7- $\bar{D}7$  system: for the D5-D5- $\bar{D}5$  configuration, there is no range of  $\ell_0/(2\pi R_{5+1})$  for which there exist the short and long solutions. Like the D5-D7- $\bar{D}7$  configuration, for the D5-D5- $\bar{D}5$  system at  $T < (2\pi R_{5+1})^{-1}$ , there is an infinite number of connected solutions when  $2\ell_0 = \pi R_{5+1}$  and none for other  $\ell_0$ 's.

For the D6-D4- $\bar{D}4$  configuration, there is always one connected solution for arbitrary values of  $\ell_0/\beta$ . Notice that the behavior of the flavor branes in the geometry of color D5 and D6-branes with  $(1+1)$ -dimensional intersections is qualitatively the same as their behavior with  $(3+1)$ -dimensional intersections.

#### 4 Energy of the configurations

As we saw in the previous section there are typically more than one solution for a given  $\ell_0/\beta$ . In fact, just to recap, for  $\ell_0/\beta$  less than a critical value there are generically three branches of solutions for  $q \leq 4$ ; one disjoint and two connected solutions. There are also an infinite number of solutions for  $q = 5$  at  $T < (2\pi R_{5+1})^{-1}$  as long as  $\ell_0 = 2\pi R_{5+1}/(r+3)$ . There are two branches of solutions for  $q = 6$  for any  $\ell_0/\beta$ ; one disjoint and one connected solution. Since there are various configurations for a particular value of  $\ell_0/\beta$ , one needs to compare their on-shell actions to determine which configuration is more energetically favorable. In this section we analyze the energy of these configurations by a combination of analytical and numerical techniques. The energy of these configurations by themselves is infinite. We regulate the energies of connected configurations by subtracting from them the energy of disjoint configurations

$$\tilde{E} = \lim_{\Lambda \rightarrow \infty} \left\{ \int_{z_*}^{\Lambda} dz z^{\frac{\sigma}{2}} \left( 1 - \frac{z_*^{\gamma} - z_*^{\sigma}}{z^{\gamma} - z^{\sigma}} \right)^{-\frac{1}{2}} - \int_1^{\Lambda} dz z^{\frac{\sigma}{2}} \right\}, \quad (4.1)$$



where  $\Lambda$  is a cutoff and the difference in energy  $E$  is related to  $\tilde{E}$  as

$$E = -\frac{\delta\beta^2}{\pi} C(q, r) u_T^{\frac{\gamma}{2}} \int d^r x \tilde{E}. \quad (4.2)$$

#### 4.1 Analytical analysis

The integral in (4.1) is complicated and as far as we know cannot be integrated analytically for generic values of  $z_*$ . However, like the integral in (3.6), there are two regions of  $z_* \rightarrow 1$  and  $z_* \gg 1$  for which we can integrate  $\tilde{E}(z_*)$  analytically. In the  $z_* \rightarrow 1$  limit, it can be shown that  $\tilde{E}$  is positive for all  $q$  and  $r$ . Indeed, let's rewrite (4.1) as follows

$$\begin{aligned} \tilde{E}_\Lambda &= \int_{z_*}^\Lambda dz z^{\frac{\sigma}{2}} \left[ \left( 1 - \frac{z_*^\gamma - z_*^\sigma}{z^\gamma - z^\sigma} \right)^{-\frac{1}{2}} - 1 \right] - \int_1^{z_*} dz z^{\frac{\sigma}{2}} \\ &= \left( \int_{z_*}^{z'_*} dz z^{\frac{\sigma}{2}} \left[ \left( 1 - \frac{z_*^\gamma - z_*^\sigma}{z^\gamma - z^\sigma} \right)^{-\frac{1}{2}} - 1 \right] - \int_1^{z_*} dz z^{\frac{\sigma}{2}} \right) \\ &\quad + \int_{z'_*}^\Lambda dz z^{\frac{\sigma}{2}} \left[ \left( 1 - \frac{z_*^\gamma - z_*^\sigma}{z^\gamma - z^\sigma} \right)^{-\frac{1}{2}} - 1 \right]. \end{aligned} \quad (4.3)$$

The last integral in (4.3) is positive for any  $z'_*$ . If  $z_* = 1 + \epsilon$ , we can choose  $z'_* = 1 + 3\epsilon$  and the difference in the bracket is estimated to be

$$\epsilon(\sqrt{6} - 2) + \epsilon \left( \log(\sqrt{2} + \sqrt{3}) - 1 \right) + o(\epsilon^2), \quad (4.4)$$

which is also positive.

Approximating (4.1) in the  $z_* \gg 1$  region yields

$$\begin{aligned} \tilde{E}_\Lambda &\sim \int_{z_*}^\Lambda dz z^{\delta+\gamma} (z^\gamma - z_*^\gamma)^{-\frac{1}{2}} - \int_1^\Lambda dz z^{\frac{\sigma}{2}}, \\ &= \left\{ \int_{z_*}^\Lambda dz z^{\delta+\gamma} (z^\gamma - z_*^\gamma)^{-\frac{1}{2}} - \int_0^\Lambda dz z^{\frac{\sigma}{2}} \right\} + \frac{2}{\sigma+2}. \end{aligned} \quad (4.5)$$

Note that in the large  $z_*$  limit,  $z_* \simeq z_0$  where  $z_0 = u_0/u_T$ . As a result, from (4.5) we see that the energy of the connected configurations approaches their zero temperature value obtained in [12]. This is expected since in this regime the connected flavor branes are very far away from the horizon hence receive little effect from it. The disjoint configuration, on the other hand, always keeps in touch with the horizon and gets a finite temperature contribution  $-\frac{2}{\sigma+2}$ . The term in the curly bracket of (4.5) is already computed in [12] in terms of Beta functions, giving an energy difference of

$$\begin{aligned} \tilde{E} &= \lim_{\Lambda \rightarrow \infty} \tilde{E}_\Lambda \\ &= \frac{1}{\gamma} z_*^{\frac{\gamma}{2} + \delta + 1} B \left[ -\frac{1}{2} - \frac{\delta+1}{\gamma}, \frac{1}{2} \right] + \frac{2}{\sigma+2}. \end{aligned} \quad (4.6)$$

Since  $z_* \gg 1$ , the last term is irrelevant in determining the sign of  $\tilde{E}$ . We see immediately that  $\tilde{E} > 0$  for  $q \geq 6$  and  $\tilde{E} < 0$  for  $q \leq 4$ . For  $q = 5$ , the Beta function vanishes,

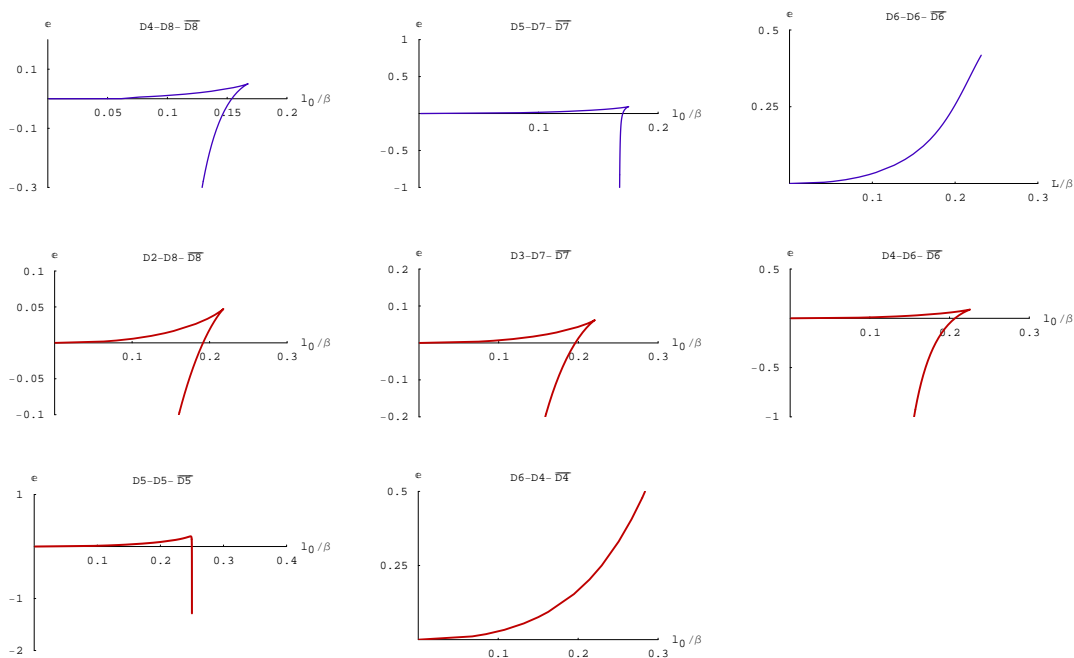


**Figure 5.** Behavior of  $\tilde{E}$  versus  $\ell_0/\beta$  obtained numerically for various  $q$ 's and intersections of interest, i.e.  $r = 1$  and  $r = 3$ . The blue plots show the behavior for  $3 + 1$  intersections whereas the red plots show the behavior for  $1 + 1$  intersections. The plots for the color D5-branes are for a fixed (inverse) temperature of  $\beta = 2\pi R_{5+1}$ .

and a more careful investigation must be made to determine the sign of  $\tilde{E}$ . It turns out that in going from (4.1) to (4.5), we have over-estimated the energy for the joined brane configurations: there is a correction with leading behavior  $\sim -z_*^{(r-1)/2}$  for large  $z_*$ . Thus, for  $q = 5$  we have  $\tilde{E} < 0$  for  $r > 1$ , while the analytic analysis is not reliable for  $r = 1$ . The analytic results for the two aforementioned limits of  $z_*$  are summarized in figure 4.

#### 4.2 Numerical results and phase transitions

For generic value of  $z_*$  the integral in (4.1) can be numerically integrated and one can plot  $\tilde{E}$  versus  $z_*$ . Instead we will numerically eliminate  $z_*$  between (3.6) and (4.1) and plot  $\tilde{E}$  versus  $\ell_0/\beta$ . The reason for doing so is that one can easily observe the transitions, say from a connected configuration to a disjoint configuration, in terms of both  $\ell_0$  and  $\beta$ . The numerical results are shown in figure 5. In the following we will analyze these graphs and determine the phases of the vacuum as one varies  $\ell_0/\beta$ .

**(3 + 1)-dimensional intersections.** As mentioned in the previous section, for  $3 + 1$ -dimensional intersections we have three configurations. Consider first the D4-D8- $\overline{D8}$  system. For  $\ell_0/\beta < (\ell_0/\beta)_{\text{cr}}^e \approx 0.154$  the short solution is more energetically favorable compared to both the disjoint and the long solutions. This corresponds to the chiral symmetry being broken. (Here  $(\ell_0/\beta)_{\text{cr}}^e$  is a critical value read off the energy diagrams in figure 5. It is different from  $(\ell_0/\beta)_{\text{cr}}$  obtained from the plots of figure 2.) Above this value (up

to  $\ell_0/\beta \approx 0.17$ ) both short and long curved solutions have more energy compared to the disjoint solution, indicating that the disjoint solution is the vacuum, hence chiral symmetry is restored and the phase transition is of first order. Thus the chiral symmetry breaking-restoration phase transition occurs at  $(\ell_0/\beta)_{\text{cr}}^e \approx 0.154$ .

For the D5-D7- $\overline{\text{D7}}$  system at  $T = (2\pi R_{5+1})^{-1}$  the behavior is surprising and to some extent more involved. On the D5-D7- $\overline{\text{D7}}$  plot in figure 5 there are two special points with  $(\ell_0)_{\text{cr}}^e \approx 0.168$  and  $0.17$  (in units of  $2\pi R_{5+1}$ ). For  $\ell_0/(2\pi R_{5+1}) < 0.168$  the disjoint solution is more energetically favorable, hence chiral symmetry in the dual theory is intact given that such a solution can represent a valid phase of the dual theory. For  $0.168 < \ell_0/(2\pi R_{5+1}) < 0.17$  there are three kinds of solutions, disjoint, short and long. It turns out that the short solution has less energy than the other two indicating that chiral symmetry is broken. For  $\ell_0/(2\pi R_{5+1}) > 0.17$  the disjoint solution becomes more energetically favorable, hence potentially chiral symmetry gets restored. For temperatures less than  $(2\pi R_{5+1})^{-1}$ , the situation is the same as the zero temperature case: there are an infinite number of connected solutions when  $3\ell_0 = \pi R_{5+1}$ , each equally energetically favored, and each of them more favored over the disjoint solution. The existence of such solutions may be rooted in the fact that the low energy theory on the color D5-branes is a non-local field theory, a little string theory. Due to the fact that in the case of background D5-brane geometry the dual field theory degrees of freedom cannot be totally decoupled from non-field theoretic degrees of freedom, it is not clear to us whether such solutions can represent a chirally-broken phase of the dual gauge theory despite the fact that, geometrically, they are smoothly connected.

For the D6-D6- $\overline{\text{D6}}$  system, the disjoint solution is always favorable, although it is not clear whether one can give a holographic interpretation that the “dual” field theory is in a chirally-symmetric phase. This is because there exists no decoupling limit suitable for holography in the case of background D6-branes.

**(1 + 1)-dimensional intersections.** For (1+1)-dimensional intersections, there are five allowed configurations. Among these the models based on background D $q$ -branes with  $q \leq 4$  exhibit similar behaviors to their counterparts with (3+1)-dimensional intersection. That is to say for sufficiently low temperatures (compared to  $1/\ell_0$ ) chiral symmetry is broken while above a critical temperature it gets restored. The critical values at which this (first order) phase transition occurs are  $(\ell_0/\beta)_{\text{cr}}^e \approx 0.191, 0.196$  and  $0.206$  for color D2, D3 and D4-branes, respectively.

The model with color D5-branes again shows some surprises. Because of the mixing between the field theoretic and non-field theoretic degrees of freedom in holography involving background D5-branes, we have no evidence that different behaviors of the flavor branes represent, via holographic point of view, either chirally-symmetric or chirally-broken phases of the dual field theory. Nevertheless, one finds the following results. At  $T = (2\pi R_{5+1})^{-1}$  and for small enough  $\ell_0$  ( $\ell_0 < (\ell_0)_{\text{cr}}^e \approx 0.2498 \times 2\pi R_{5+1}$ ) the disjoint solution is preferred. Increasing  $\ell_0$  up to  $\ell_0/(2\pi R_{5+1}) < 0.251$  will result in a phase where the connected solution is favorable. This phase appears in our plot because we put a cutoff of  $\Lambda = 5$  to regulate the energy integral. Increasing the cutoff will decrease the range of  $\ell_0$  for which this phase exists. It is plausible that in the  $\Lambda \rightarrow \infty$  limit this phase disappears although our numerics

does not allow us to check this explicitly. Sticking for now with the cutoff we chose, if one increases  $\ell_0$  further, there will be another phase transition to a phase where the disjoint solution becomes favored. Due to space limitations, the resolution of the D5-D5- $\bar{D}5$  plot in figure 5 does not allow one to see all these phases. For temperatures less than  $(2\pi R_{5+1})^{-1}$ , like the zero temperature case, there are an infinite number of connected solutions for  $\ell_0 = \pi R_{5+1}/2$ , each equally energetically favored, and none for other  $\ell_0$ 's. Each of these connected solutions is more favored over the disjoint solution. For the D6-D4- $\bar{D}4$  system, there is no phase transition and it is always the disjoint solution which is energetically favorable.

## 5 Transverse intersections at finite temperature with compact $x^q$

An interesting property of the models we are studying here is that when  $x^q$  is compact the scale of chiral symmetry breaking is generically different from the scale of confinement which results in additional phases. For example, for the Sakai-Sugimoto model at finite temperature, it was shown [10] that there exists an intermediate phase where the system is deconfined while chiral symmetry is broken.

At finite temperature and  $x^q$  direction being compact (with a radius of  $R_c$ ), there are three geometries where the topology of the  $t - x^q$  submanifold is  $S^1 \times S^1$ . One is a geometry which has the metric

$$ds^2 = \left(\frac{u}{R_{q+1}}\right)^{\frac{7-q}{2}} \left(dt^2 + d\vec{x}^2 + g(u)(dx^q)^2\right) + \left(\frac{u}{R_{q+1}}\right)^{-\frac{7-q}{2}} \left(\frac{du^2}{g(u)} + u^2 d\Omega_{8-q}^2\right), \quad (5.1)$$

with

$$g(u) = 1 - \left(\frac{u_{\text{KK}}}{u}\right)^{7-q}. \quad (5.2)$$

We will call this geometry the thermal geometry. Although the Euclidean time period  $\beta$  is arbitrary in this geometry, the  $x^q$ -circle cannot have arbitrary periodicity. In order for this geometry to be smooth at  $u = u_{\text{KK}}$  in the  $x^q - u$  submanifold, one has to have

$$\Delta x^q = \beta_c = \frac{4\pi}{7-q} \left(\frac{R_{q+1}}{u_{\text{KK}}}\right)^{\frac{7-q}{2}} u_{\text{KK}}, \quad (5.3)$$

where we have defined  $\beta_c = 2\pi R_c$ . Although we do not specify the  $q$ -dependence of  $\beta_c$  and  $R_c$ , one should keep in mind that they depend on  $u_{\text{KK}}$  and  $R_{q+1}$  differently through (5.3) depending on what value for  $q$  is given. There is another geometry whose metric takes the form

$$ds^2 = \left(\frac{u}{R_{q+1}}\right)^{\frac{7-q}{2}} \left(dt^2 + d\vec{x}^2 + (dx^q)^2\right) + \left(\frac{u}{R_{q+1}}\right)^{-\frac{7-q}{2}} \left(du^2 + u^2 d\Omega_{8-q}^2\right). \quad (5.4)$$

There is also the black brane geometry which is basically the same as (2.2) but with  $x^q$  compact, and has the (Euclidean) metric

$$ds^2 = \left(\frac{u}{R_{q+1}}\right)^{\frac{7-q}{2}} \left(f(u)dt^2 + d\vec{x}^2 + (dx^q)^2\right) + \left(\frac{u}{R_{q+1}}\right)^{-\frac{7-q}{2}} \left(\frac{du^2}{f(u)} + u^2 d\Omega_{8-q}^2\right), \quad (5.5)$$

where

$$f(u) = 1 - \left(\frac{u_T}{u}\right)^{7-q}. \quad (5.6)$$

In this geometry the  $x^q$ -circle has arbitrary periodicity whereas  $\beta$  is fixed by

$$\beta = \frac{4\pi}{7-q} \left(\frac{R_{q+1}}{u_T}\right)^{\frac{7-q}{2}} u_T. \quad (5.7)$$

For all three geometries, the dilaton  $\phi$ , and the  $q$ -form RR-flux  $F_q$  are given in (2.6); see the appendix for more details. Also,  $R_{q+1}$  is given in (2.4).

The three geometries whose line elements are given in (5.1), (5.4) and (5.5) are saddle points of either type IIA or type IIB Euclidean path integral. For a given temperature, one needs to compare their (regularized) free energies to determine which solution dominates the path integral. We have calculated the free energies of these solutions in the appendix. For  $q \leq 4$ , both the thermal and the black brane geometries have less free energy compared to the geometry in (5.4), and this result is independent of temperature. So, to determine the lowest energy saddle point we need to compare the free energies of (5.1) and (5.5). The difference in their free energies is given by

$$S_{\text{thermal}} - S_{\text{black brane}} = \frac{9-q}{g_s^2} V_9 \left(\frac{4\pi}{7-q} R_{q+1}^{\frac{1}{2}(7-q)}\right)^{2\frac{7-q}{5-q}} \left(\beta^{2\frac{q-7}{5-q}} - \beta_c^{2\frac{q-7}{5-q}}\right), \quad (5.8)$$

where  $V_9 = \beta\beta_c \text{Vol}(S^{8-q})\text{Vol}(\mathbb{R}^{q-1})$  where we set  $l_s = 1$ . Thus the thermal geometry (5.1) dominates when  $\beta > 2\pi R_c$  whereas for  $\beta < 2\pi R_c$  it is the black brane geometry (5.5) which gives the dominant contribution to the Euclidean path integral. This phase transition which happens at  $\beta = \beta_c$  is the holographic dual of confinement-deconfinement phase transition in the corresponding dual gauge theories [6].

For  $q = 6$ , again, both the thermal and black brane geometries have less free energy compared to the geometry in (5.4). The difference in free energies for the geometries in (5.1) and (5.5) is given by

$$S_{\text{thermal D6}} - S_{\text{black D6-brane}} = \frac{3V_9}{16\pi^2 g_s^2 R_{6+1}} (\beta^2 - \beta_c^2), \quad (5.9)$$

where  $V_9 = \beta\beta_c \text{Vol}(S^2)\text{Vol}(\mathbb{R}^5)$ . So, (5.9) indicates a phase transition at  $\beta = 2\pi R_c$ . Unlike the  $q \leq 4$  cases, for  $q = 6$  the thermal geometry (5.1) dominates for  $\beta < 2\pi R_c$  whereas for  $\beta > 2\pi R_c$  the black brane geometry (5.5) dominates.

For  $q = 5$ , one needs to consider more possibilities. For  $\beta = 2\pi R_{5+1}$ , there are two cases: either  $\beta_c = 2\pi R_{5+1}$  or  $\beta_c \neq 2\pi R_{5+1}$ . For  $\beta_c = 2\pi R_{5+1}$ , both (5.1) and (5.5) are more favored over the geometry whose metric is given in (5.4). The difference in free energies of (5.1) and (5.5) is

$$S_{\text{thermal D5}} - S_{\text{black D5-brane}} = \frac{4}{g_s^2} V_9 (u_T^2 - u_{\text{KK}}^2), \quad \text{at} \quad \beta_c = 2\pi R_{5+1}. \quad (5.10)$$

where  $V_9 = \beta\beta_c \text{Vol}(S^3)\text{Vol}(\mathbb{R}^4)$ . For  $\beta_c \neq 2\pi R_{5+1}$ , on the other hand, the two saddle points with the same asymptotics are the black brane geometry and the geometry in (5.4). In this case, the black brane geometry is the dominant one

$$\Delta S = \frac{4}{g_s^2} V_9 u_T^2 > 0. \quad (5.11)$$

There are also two possibilities when  $\beta \neq 2\pi R_{5+1}$ . If  $\beta_c \neq 2\pi R_{5+1}$ , the only saddle point consistent with the asymptotics is (5.4) which determines the vacuum. If, on the other hand,  $\beta_c = 2\pi R_{5+1}$ , there are two geometries with the same asymptotics, thermal and the one given in (5.4). The thermal geometry is dominant because

$$\Delta S = -\frac{4}{g_s^2} V_9 u_{\text{KK}}^2 < 0. \quad (5.12)$$

With  $x^q$  being compact, the flavor branes are now sitting at two points separated by a distance  $\ell_0$  on the  $x^q$ -circle. Note that there is no reason for the flavors branes to be located at the antipodal points on the circle. As before, we consider the transverse intersections of the flavor and the color branes, and choose the same embeddings and boundary conditions for the flavor branes as we did in (2.10) and (2.11) except that now  $\ell_0 \leq \pi R_c$ . In what follows, we will focus on  $q \leq 4$  cases and consider both low and high temperature phases of the background. In particular, we would like to know whether there always exists a range of temperature above the deconfinement temperature where chiral symmetry is broken.

### 5.1 Behavior at high and low temperatures

For temperatures above the deconfinement temperature  $\beta_c$  the profile of the flavor branes takes essentially the same form as it did when  $x^q$  was non-compact, hence, indicating the existence of short and long (smoothly) connected solutions. Note that when  $x^q$  is compact, for a fixed  $\ell_0$ , there is now a lower bound on  $\ell_0/\beta$  set by the deconfinement temperature. For completeness, we have plotted  $\ell_0/\beta$  versus  $z_*$  ( $z_*$  being the radial position at which the brane and anti-brane smoothly join) in figure 6. The lower dotted line in each plot represents the deconfinement temperature. As an example, we chose it to be at  $\beta_c = 10\ell_0$ . The upper dotted line shows chiral symmetry breaking-restoration phase transition which comes from comparing the energies of connected and disjoint solutions. One can show, using energy considerations, that below the upper dotted line chiral symmetry is broken in a deconfined phase via short connected solution while it is restored above the line (where we have deconfinement with chiral symmetry restoration).

In the low temperature regime where the system is in a confined phase, the DBI action for the flavor branes in the thermal background (5.1) now reads (with gauge fields set equal to zero)

$$S_{\text{DBI}} = \beta C(q, r) \int d^r x dx^q u^{\frac{\gamma}{2}} \left[ g(u) + \frac{1}{g(u)} \left( \frac{u}{R_{q+1}} \right)^{2\delta} u'^2 \right]^{\frac{1}{2}}, \quad (5.13)$$

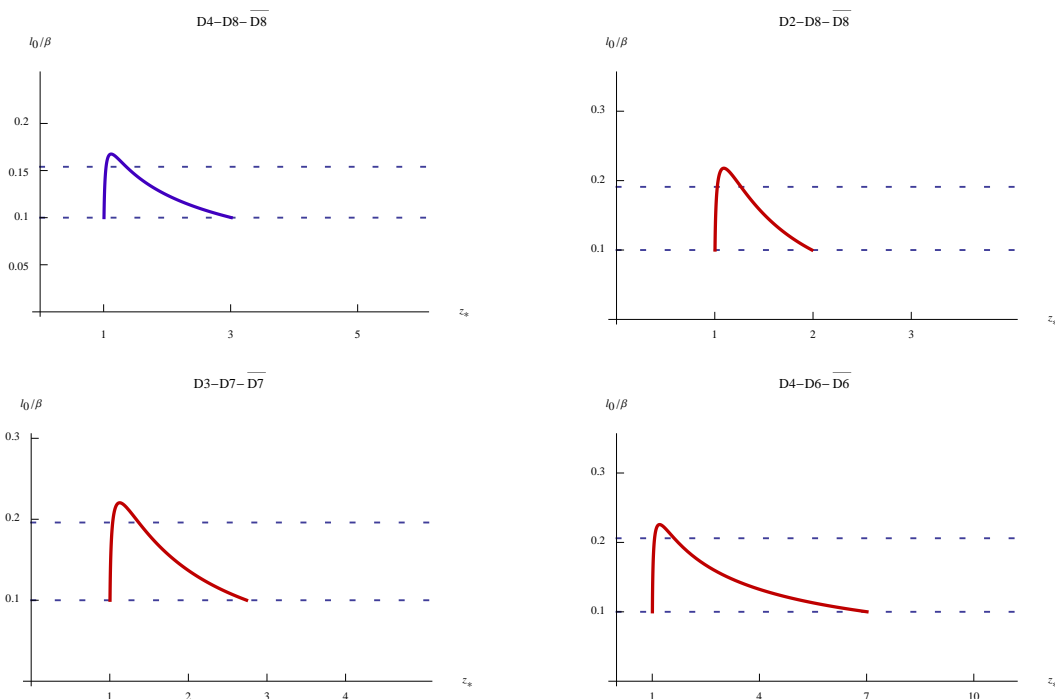


**Figure 6.** Behavior of  $\ell_0/\beta$  versus  $z_*$  above the deconfinement temperature for  $q = 2, 3, 4$ . The lower dotted line represents a transition to the confined phase whereas the upper dotted line represents chiral symmetry breaking-restoration phase transition.

where  $C(q, r)$ ,  $\gamma$  and  $\delta$  have all been defined in (2.14). The equation of motion for the profile is now

$$u^{\frac{\gamma}{2}} g(u) \left[ g(u) + \frac{1}{g(u)} \left( \frac{u}{R_{q+1}} \right)^{2\delta} u'^2 \right]^{-\frac{1}{2}} = w_0^{\frac{\gamma}{2}}, \quad (5.14)$$

with  $w_0$  parameterizing the solutions. There exists a solution with  $w_0 = 0$  representing disjoint  $Dp$  and  $\overline{Dp}$ -branes descending down to  $u = u_{\text{KK}}$ . For  $w_0 \neq 0$ , solving (5.14) for  $u'$  yields

$$u'^2 = \frac{1}{w_0^\gamma} \left( \frac{u}{R_{q+1}} \right)^{-2\delta} g(u)^2 \left( u^\gamma g(u) - w_0^\gamma \right). \quad (5.15)$$

Denoting the possible turning point(s) by  $w_*$ , analysis of (5.15) shows that  $u \geq w_* > u_{\text{KK}}$ , with  $w_*$  satisfying

$$w_*^\gamma - w_*^\sigma u_{\text{KK}}^{-2\delta} - w_0^\gamma = 0, \quad (5.16)$$

where  $\sigma$  has been defined as before. Integrating (5.15) gives

$$x^q(y) = -\frac{\delta}{2\pi} \beta_c (y_*^\gamma - y_*^\sigma)^{\frac{1}{2}} \int_{y_*}^y \left( \tilde{y}^{-2\delta} - 1 \right)^{-1} \left( \tilde{y}^\gamma - \tilde{y}^\sigma - (y_*^\gamma - y_*^\sigma) \right)^{-\frac{1}{2}} d\tilde{y}, \quad (5.17)$$

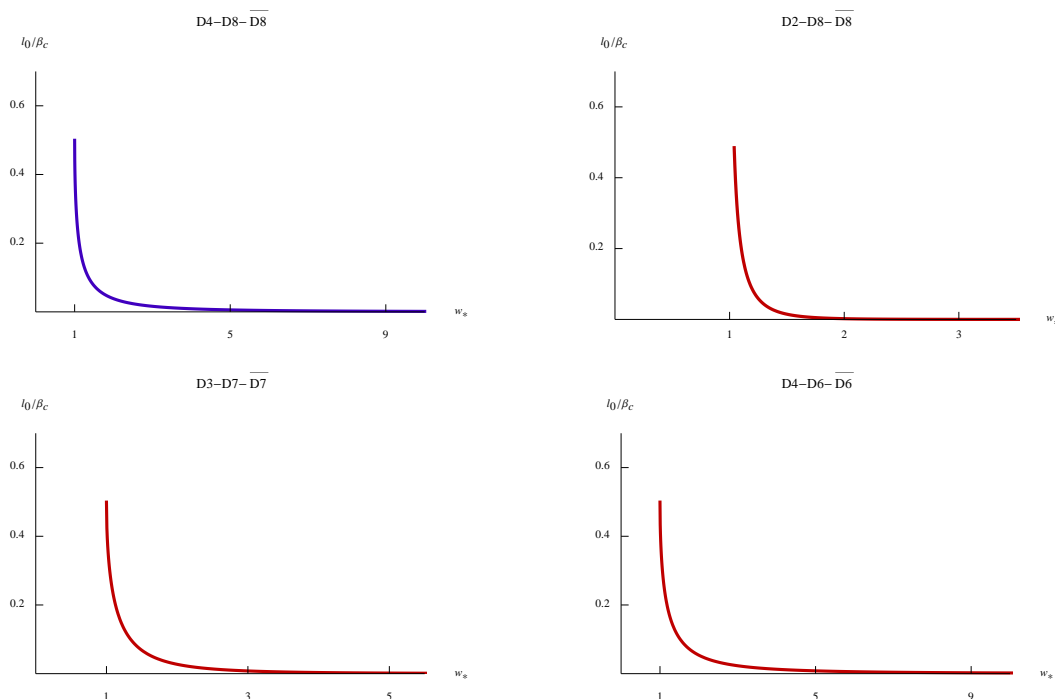


**Figure 7.** Behavior of  $\ell_0/\beta_c$  versus  $w_*$  for  $q = 2, 3, 4$ .

where we have defined  $y = (u/u_{\text{KK}}) \in (1, \infty)$ , and  $y_* = w_*/u_{\text{KK}}$ . Using (5.17) we can relate  $y_*$  to  $\ell_0$

$$\frac{\ell_0}{\beta_c} = -\frac{\delta}{\pi} (y_*^\gamma - y_*^\sigma)^{\frac{1}{2}} \int_{y_*}^{\infty} (y^{-2\delta} - 1)^{-1} (y^\gamma - y^\sigma - (y_*^\gamma - y_*^\sigma))^{-\frac{1}{2}} dy. \quad (5.18)$$

The analysis of  $\ell_0/\beta_c$  as a function of  $y_*$  determines the number of solutions.  $\ell_0/\beta_c$  versus  $y_*$  has been numerically plotted in figure 7 for intersections of interest and for  $q = 2, 3, 4$ . As it is seen from figure 7, there is always one smoothly connected solution (as well as a disjoint solution). The red and blue plots represent smoothly connected solutions for (1+1)-dimensional and (3+1)-dimensional intersections, respectively.

For the energy of the connected solutions, one obtains

$$E = -\frac{\delta\beta}{\pi} \beta_c C(q, r) u_{\text{KK}}^{\frac{\gamma}{2}} \int dx^r \tilde{E}, \quad (5.19)$$

where

$$\tilde{E} = \lim_{\Lambda \rightarrow \infty} \left\{ \int_{y_*}^{\Lambda} dy y^{\frac{\sigma}{2}} (1 - y^{2\delta})^{-\frac{1}{2}} \left( 1 - \frac{y_*^\gamma - y_*^\sigma}{y^\gamma - y^\sigma} \right)^{-\frac{1}{2}} - \int_1^{\Lambda} dy (1 - y^{2\delta})^{-\frac{1}{2}} y^{\frac{\sigma}{2}} \right\}, \quad (5.20)$$

and  $\Lambda$  is a cutoff. Like the previous sections, one can numerically eliminate  $y_*$  between (5.18) and (5.20) and plot  $\tilde{E}$  versus  $\ell_0/\beta_c$ . Although we have not shown the plots here, one can check (numerically) that the smoothly connected solutions are always more energetically favorable compared to the disjoint solutions.

The plots in figure 7 not only show the existence of a unique smoothly connected solution (for the confined phase) but also indicate a big difference for the behavior of



the flavor branes below and above the confinement-deconfinement phase transition. For example consider the plot for D3- D7- $\overline{D7}$  system. Each point on the plot represents a unique curved solution for which increasing the temperature (up to the deconfinement temperature  $\beta_c$ ) will have no effect on the shape of the U-shaped flavor branes. That is to say that changing the temperature will not cause the flavor D7- $\overline{D7}$ -branes to join either closer to  $u_{KK}$  or farther away from it. Once  $\ell_0$  and  $\beta_c$  are specified, the shape of the brane stays the same independent of the variation of the temperature up to the deconfinement temperature. The behavior just mentioned is significantly different from the behavior of the flavor branes at high temperatures (where they are in black brane backgrounds). For a fixed  $\ell_0$ , each point on the plot of D3-D7- $\overline{D7}$  system in figure 7 represents one (or two) smoothly connected solution(s) for only a specific temperature. Varying the temperature will now change the shape of the connected flavor branes and force them to go either closer to the horizon or stay farther away from it.

There is another difference which is worthy of mentioning here. At the temperature for which the confinement-deconfinement phase transition occurs, namely at  $\beta = \beta_c$ ,  $u_{KK} = u_T$ . For a fixed  $\ell_0$ , flavor branes at temperatures above  $\beta_c$  join at a radial point closer to  $u_{KK} = u_T$  than the same flavor branes placed at temperatures below  $\beta_c$ .

## 6 Discussion

In this paper, we analyzed some aspects of transversely-intersecting  $Dq$ - $Dp$ - $\overline{Dp}$ -branes at finite temperature. In particular, we mapped out different vacuum configurations which can holographically be identified with chiral symmetry breaking (or restoration) phase of their holographic dual theories. Although we showed that generically the long connected solutions are less energetically favorable compared to the short connected solutions we did not discuss their stability against small perturbations. Presumably a stability analysis along the lines of [19] can be done to show that the long connected solution is unstable against small perturbations. The analysis presented here can be generalized in various directions. For example, one can add a chemical potential to the setup and look for new phases as was done in some specific models in [20–23], or consider the system at background electric and magnetic fields [24–26] and study the conductivity of the system or the effect of the magnetic field on the chiral symmetry-restoration temperature. We hope to come back to these interesting issues in future.

Also, our analysis was entirely based on the DBI action for the flavor  $Dp$ - $\overline{Dp}$ -branes. In transversely-intersecting D-branes, working with just the DBI (plus the Chern-Simons part of the) action misses, from holographic perspectives, an important part of the physics, namely the vev of the fermion bilinear as an order parameter for chiral symmetry breaking. To determine the fermion bilinear from the holographic point of view there should be a mode propagating in the bulk geometry such that asymptotically its normalizable mode can be identified with the vev of the fermion bilinear. The DBI plus the Chern-Simons action cannot give rise to the mass of the localized chiral fermions either. Note that for transverse intersections one cannot write an explicit mass term for the fermions of the intersections because there is no transverse space common to both the color and the flavor branes. So it is not possible to stretch an open string between the color and flavor branes in

the transverse directions. Therefore, the fermion mass must be generated dynamically. It has been argued in [8] that including the dynamics of an open string stretched between the flavor branes into the analysis will address the question of how one can compute fermion mass and bilinear vev in these holographic models. More concretely, the scalar mode of this open string which transforms as bifundamental of  $U(N_f) \times U(N_f)$  has the right quantum numbers to be potentially holographically dual to the fermion mass and condensation.

Recently, the authors of [28–30] shed light on this issue by starting with the so-called tachyon-DBI action [27] claimed to correctly incorporate the role of the open string scalar mode, the tachyon, in a system of separated  $Dp\text{-}\overline{Dp}$ -branes. In fact, it was shown in [29, 30] that for the Sakai-Sugimoto model at zero temperature, the open string tachyon will asymptotically have a normalizable as well as a non-normalizable mode. They identified the normalizable mode with the vev of the fermion bilinear (order parameter for chiral symmetry breaking) and the non-normalizable mode with the fermion mass. It is not hard to generalize the calculations of [29, 30] to include all transversely-intersecting  $Dq\text{-}Dp\text{-}\overline{Dp}$  systems at zero temperature where one finds that there always exist both normalizable and non-normalizable modes for the asymptotic behavior of the tachyon, and in the bulk of the geometry the tachyon condenses roughly at the same radial point where the flavor branes smoothly join [31]. The calculation of the fermion mass and condensate for transversely-intersecting  $Dq\text{-}Dp\text{-}\overline{Dp}$  systems at finite temperature requires not only considering the tachyon-DBI action of [27] in the black brane background of (2.2) but also calculating the tachyon potential as a function of the temperature. In the case of a coincident brane and anti-brane in flat background, a partial result for such a calculation was given in [32] (see also [33]). Some attempts in generalizing the results of [32, 33] for separated brane-anti-branes (at least in the case of separated  $D8\text{-}\overline{D8}$  in flat space) has recently started in [34]. For our purpose of extracting information about fermion mass and condensate, knowing the dependence of the tachyon potential for separated flavor  $Dp\text{-}\overline{Dp}$ -branes seems crucial. Ignoring the temperature dependence on tachyon potential at zeroth order yields unsatisfactory results: It gives rise to the same results as one would have obtained in the zero temperature case [31]. We know that this is not the right behavior because at zero temperature there is no chiral phase transition.

**Note added in version two.** There are now two more interesting (and closely related) proposals on how to compute the fermion mass and condensates in transversely-intersecting D-branes. One proposal is based on an open wilson line operator whose vev gives the condensate [35] (see also [36, 37] for generalizations) and the other [38] is based on a D6-brane, in the case of the Sakai-Sugimoto model, ending on the flavor  $D8\text{-}\overline{D8}$ -branes. It would be interesting to understand the relations between these two proposals and the one based on the open string tachyon.

## Acknowledgments

We would like to thank P. Argyres, S. Baharian, O. Bergman, and especially J. F. Vázquez-Poritz for helpful discussions and comments. This work is supported by DOE grant DE-FG02-91ER40709.

## A Free energies of possible bulk backgrounds

Following [10] we use the notation adopted in [39] to compute the free energy of possible finite temperature Dq-brane backgrounds for both compact and non-compact  $x^q$ -direction. We first consider the case of compact  $x^q$  and as a warm-up first do the computation for D6-branes, then generalize it to Dq-branes.

### A.1 Compact $x^q$

**D6-branes.** Consider the bosonic part of type IIA supergravity action (in Euclidean signature and) in string frame

$$\begin{aligned}
 S &= -(S_{\text{EH}} + S_\phi + S_{\text{RR}} + S_{\text{NS}}), \\
 &= - \int e^{-2\phi} \sqrt{g} (\mathcal{R} + 4\partial\phi\partial\phi) + \frac{1}{2} \sum_q \int F_{(q+2)} \wedge *F_{(q+2)} + \frac{1}{2} \int e^{-2\phi} H_{(3)} \cdot \wedge *H_{(3)}. \quad (\text{A.1})
 \end{aligned}$$

Having the near horizon geometry of D6-branes in mind, we choose the following (radial) ansatz for the metric and RR 7-form  $C_{(7)}$

$$l_s^{-2} ds^2 = d\tau^2 + e^{2\lambda(\tau)} dx_{\parallel}^2 + e^{2\tilde{\lambda}(\tau)} dx_c^2 + e^{2\nu(\tau)} d\Omega_2^2, \quad (\text{A.2})$$

$$C_{(7)} = A dx^1 \wedge \dots \wedge dx^5 \wedge dx^{6-c} \wedge dx^c, \quad (\text{A.3})$$

where  $d\Omega_2^2$  is the line element of the unit two-sphere. Certainly the backgrounds we considered in this paper can all be put into the form of our ansatz (A.2). Here  $\tau$  is the radial coordinate,  $x_{\parallel}$  are 6 (out of 7) worldvolume directions,  $x_c$  plays the role of time in black D6-brane geometry and  $x^6$  in thermal geometry. From now on we set  $l_s = 1$ . It could be restored into our results by dimensional analysis.

The equation of motion of  $C_{(7)}$  has the solution

$$\dot{A} e^{-6\lambda - \tilde{\lambda} + 2\nu} = \text{const}, \quad (\text{A.4})$$

where the dot represents the derivative with respect to  $\tau$ . Substituting (A.4) into (A.1), the RR part of the action reads

$$-S_{\text{RR}} = \int Q^2 e^{6\lambda + \tilde{\lambda} - 2\nu} d\tau, \quad (\text{A.5})$$

where  $Q^2$  is an integration constant. It is more convenient to define a new radial coordinate  $d\rho = -e^\varphi d\tau$ , where

$$\varphi = 2\phi - 6\lambda - \tilde{\lambda} - 2\nu, \quad (\text{A.6})$$

in terms of which (A.5) reads

$$-S_{\text{RR}} = - \int Q^2 e^{6\lambda + \tilde{\lambda} - 2\nu - \varphi} d\rho. \quad (\text{A.7})$$

Note that  $\sqrt{g} e^{-2\phi} d\tau = -e^{-2\varphi} d\rho$  by which the dilaton action is easily computed to give

$$-S_\phi = \int 4\phi'^2 d\rho, \quad (\text{A.8})$$

where prime denotes the derivative with respect to  $\rho$ . With our metric ansatz (A.2), the Ricci scalar is

$$\mathcal{R} = 2e^{-2\nu} - 42\dot{\lambda}^2 - 2\ddot{\lambda}^2 - 6\dot{\nu}^2 - 12\dot{\lambda}\ddot{\lambda} - 24\dot{\lambda}\dot{\nu} - 4\ddot{\lambda}\dot{\nu} - 12\ddot{\lambda} - 2\ddot{\nu} - 4\ddot{\nu}. \quad (\text{A.9})$$

Thus, expressed in terms of the  $\rho$  coordinate, the Einstein-Hilbert action becomes

$$\begin{aligned} -S_{\text{EH}} &= \int \mathcal{R}e^{-2\varphi} d\rho, \\ &= \int \left[ 2e^{-2\nu-2\varphi} - 42\lambda'^2 - 2\tilde{\lambda}'^2 - 6\nu'^2 - 12\lambda'\tilde{\lambda}' - 24\lambda'\nu' - 4\tilde{\lambda}'\nu' - 12(\lambda'' + \lambda'\varphi') \right. \\ &\quad \left. - 2(\tilde{\lambda}'' + \tilde{\lambda}'\varphi') - 4(\nu'' + \nu'\varphi') \right] d\rho. \end{aligned} \quad (\text{A.10})$$

Note that the terms with double primes are total derivatives and are cancelled by adding the Gibbons-Hawking term to (A.10). Using (A.6),  $S_{\text{EH}}$  and  $S_\phi$  add up to give the following simple expression

$$-S_{\text{EH}} - S_\phi = \int \left( 2e^{-2\nu-2\varphi} - 6\lambda'^2 - \tilde{\lambda}'^2 - 2\nu'^2 + \varphi'^2 \right) d\rho. \quad (\text{A.11})$$

Putting everything together, the total action reads

$$S = \int \left( 2e^{-2\nu-2\varphi} - 6\lambda'^2 - \tilde{\lambda}'^2 - 2\nu'^2 + \varphi'^2 - Q^2 e^{6\lambda+\tilde{\lambda}-2\nu} \right) d\rho. \quad (\text{A.12})$$

The equations of motion are

$$\lambda'' = \frac{Q^2}{2} e^{-2\phi+12\lambda+2\tilde{\lambda}}, \quad (\text{A.13})$$

$$\tilde{\lambda}'' = \frac{Q^2}{2} e^{-2\phi+12\lambda+2\tilde{\lambda}}, \quad (\text{A.14})$$

$$\nu'' = e^{-4\phi+12\lambda+2\tilde{\lambda}+2\nu} - \frac{Q^2}{2} e^{-2\phi+12\lambda+2\tilde{\lambda}}, \quad (\text{A.15})$$

$$\phi'' = \frac{3Q^2}{2} e^{-2\phi+12\lambda+2\tilde{\lambda}}, \quad (\text{A.16})$$

where  $\varphi$  has been replaced by  $\phi$  using (A.6). Defining  $\Phi = -2\phi + 12\lambda + 2\tilde{\lambda}$ , (A.13), (A.14) and (A.16) give

$$\Phi'' = 4Q^2 e^\Phi, \quad (\text{A.17})$$

with the following solution

$$\Phi = -2 \ln \left( \frac{\sqrt{2}Q}{CC_1} \sinh C_1 \rho \right) - 2 \ln C. \quad (\text{A.18})$$

The last term in (A.18) is there just for convenience. Going back to (A.13), (A.14) and (A.16) and solving for  $\lambda$ ,  $\tilde{\lambda}$  and  $\phi$ , one obtains

$$\lambda = -\frac{1}{4} \ln \left( \frac{\sqrt{2}Q}{g_s C_1} \sinh C_1 \rho \right) + C_2^\lambda \rho, \quad (\text{A.19})$$

$$\tilde{\lambda} = -\frac{1}{4} \ln \left( \frac{\sqrt{2}Q}{g_s C_1} \sinh C_1 \rho \right) + C_2^{\tilde{\lambda}} \rho, \quad (\text{A.20})$$

$$\phi = -\frac{3}{4} \ln \left( \frac{\sqrt{2}Q}{g_s C_1} \sinh C_1 \rho \right) + C_2^\phi \rho + \ln g_s, \quad (\text{A.21})$$

with  $6C_2^\lambda + C_2^{\tilde{\lambda}} - C_2^\phi = 0$ . The constants  $C_1$ ,  $C_2^\lambda$ ,  $C_2^{\tilde{\lambda}}$  and  $C_2^\phi$  are to be determined. Defining  $\Phi_0 = \Phi + 2 \ln g_s$ , the equation of motion for  $\nu$  becomes

$$\nu'' = e^{\frac{\Phi_0}{4} - 2C_2^\phi \rho - 4 \ln g_s + 2\nu} - \frac{1}{2} Q^2 e^\Phi. \quad (\text{A.22})$$

If we take  $2\nu = \frac{3}{4\Phi_0} + 2C_2^\phi \rho + C_\nu$ , the above equation is satisfied if

$$C_\nu = \ln 2Q^2 g_s^2.$$

Thus, we obtain

$$\nu = -\frac{3}{4} \ln \left( \frac{\sqrt{2}Q}{g_s C_1} \sinh C_1 \rho \right) + C_2^\phi \rho + \ln \sqrt{2} Q g_s. \quad (\text{A.23})$$

In what follows we show that the near horizon geometry of non-extremal D6-branes satisfies (A.19), (A.20), (A.21). This geometry takes the form

$$ds^2 = f^{-1/2} (dx_{\parallel}^2 + h dx_c^2) + f^{1/2} \left( \frac{1}{h} du^2 + u^2 d\Omega_2^2 \right), \quad (\text{A.24})$$

$$e^{-2\phi} = g_s^{-2} f^{3/2}, \quad (\text{A.25})$$

with

$$f = \frac{g_s N_c}{2l_s u}, \quad \text{and} \quad h = 1 - \frac{u_c}{u}, \quad (\text{A.26})$$

where  $u_c$  is either  $u_T$  or  $u_{\text{KK}}$  (or zero for the geometry given in (5.4)). The  $u$  coordinate is not the same as  $\rho$ . Their relation can be inferred from (A.19) and (A.20), and is given by

$$e^{2(\tilde{\lambda} - \lambda)} = e^{2\rho(C_2^{\tilde{\lambda}} - C_2^\lambda)} = h, \quad (\text{A.27})$$

yielding

$$\begin{aligned} \rho &= \frac{1}{2\Delta C_2} \ln h, \\ d\rho &= \frac{u_c}{2u^2 \Delta C_2} \frac{1}{h} du, \end{aligned} \quad (\text{A.28})$$

where  $\Delta C_2 = C_2^{\tilde{\lambda}} - C_2^\lambda$ . Computing  $e^{2\lambda}$  from (A.19), we have

$$\begin{aligned}
 e^{2\lambda} &= \frac{e^{2C_2^\lambda \rho}}{\sqrt{\left(\frac{\sqrt{2}Q}{g_s C_1}\right) \sinh C_1 \rho}}, \\
 &= \sqrt{\frac{\sqrt{2}C_1 g_s}{Q}} \frac{h^{\frac{C_2^\lambda}{\Delta C_2}}}{\sqrt{h^{\frac{C_1}{2\Delta C_2}} - h^{\frac{-C_1}{2\Delta C_2}}}}, \\
 &= \sqrt{\frac{\sqrt{2}C_1 g_s}{Q}} \frac{h^{\frac{C_2^\lambda}{\Delta C_2} - \frac{C_1}{4\Delta C_2}}}{\sqrt{1 - h^{\frac{-C_1}{\Delta C_2}}}}. \tag{A.29}
 \end{aligned}$$

To match  $e^{2\lambda}$  in (A.29) with  $f^{1/2}$ , one has to impose  $-C_1 = \Delta C_2$  and  $C_1 = 4C_2^\lambda$ , or

$$C_1 = 4C_2^\lambda; \quad C_2^{\tilde{\lambda}} = -3C_2^\lambda. \tag{A.30}$$

Thus, we have

$$e^{2\lambda} = \sqrt{\frac{\sqrt{2}C_1 g_s}{Q}} \frac{u}{u_c} \equiv \left(\frac{2l_s u}{g_s N}\right)^{1/2} \Rightarrow C_2^\lambda = \frac{Q u_c l_s}{2\sqrt{2}g_s^2 N}. \tag{A.31}$$

Taking  $C_2^\phi = 3C_2^\lambda$ , we can match the dilaton with the dilaton of the D6-brane solution (A.25)

$$e^{2\phi} = e^{6\lambda + 2\ln g_s} = g_s^2 \left(\frac{2l_s u}{g_s N_c}\right)^{3/2}. \tag{A.32}$$

Furthermore, from (A.23), we have

$$e^{2\nu} = 2Q^2 g_s^2 e^{6\lambda} = 2Q^2 g_s^2 \left(\frac{2l_s u}{g_s N_c}\right)^{3/2} \equiv \left(\frac{g_s N}{2l_s u}\right)^{1/2} u^2 \Rightarrow N = 2\sqrt{2}Q l_s \tag{A.33}$$

The final check is the  $g_{uu}$  component of the metric. To do that, we first need to compute  $e^{-2\varphi}$  which turns out to be

$$\begin{aligned}
 e^{-2\varphi} &= e^{-4\phi + 12\lambda + 2\tilde{\lambda} + 6\nu}, \\
 &= e^{14\lambda - 8C_2^\lambda \rho + 4\ln(\sqrt{2}Q g_s) - 4\ln g_s}, \\
 &= \left(\frac{2l_s u}{g_s N}\right)^{7/2} h(\sqrt{2}Q)^4. \tag{A.34}
 \end{aligned}$$

Hence,

$$\begin{aligned}
 d\tau^2 &= e^{-2\varphi} d\rho^2, \\
 &= \left(\frac{2l_s u}{g_s N}\right)^{7/2} h(\sqrt{2}Q)^4 \frac{u_c^2}{4u^4 (16(C_2^\lambda)^2)} \frac{1}{h^2}, \\
 &= \left(\frac{g_s N_c}{2l_s u}\right)^{1/2} \frac{1}{h}, \tag{A.35}
 \end{aligned}$$

where we have used (A.31) and (A.33) to simplify the expression. Thus, the near horizon geometry of  $N_c$  D6-branes is indeed a solution to type IIA supergravity equations of motion.

It is now straightforward to plug (A.19), (A.20), (A.21) and (A.23) into (A.12) to obtain the on-shell action (free energy). Changing the coordinate from  $\rho$  coordinate to  $u$  and being careful about the fact that  $d\rho/du$  is negative, we obtain

$$S = -V_9 \int_{u_c}^{\infty} \left\{ \left( -6\lambda'^2 - \tilde{\lambda}'^2 - 2\nu'^2 + \varphi'^2 \right) \frac{du}{d\rho} + \left( 2e^{-2\nu-2\varphi} - Q^2 e^{6\lambda+\tilde{\lambda}-2\nu} \right) \frac{d\rho}{du} \right\} du \quad (\text{A.36})$$

$$= \frac{3}{g_s^2} V_9 \int_{u_c}^{\Lambda} du = \frac{3}{g_s^2} V_9 (\Lambda - u_c). \quad (\text{A.37})$$

where in the first line prime denotes the  $u$ -derivative, and  $V_9$  is the volume (in units of string length which we set equal to one) of space transverse to  $u$ :  $V_9 = \beta \text{Vol}(S_{x^q}^1) \text{Vol}(S^2) \text{Vol}(\mathbb{R}^5)$ . The free energy is infinite. That is why we put a cutoff  $u = \Lambda$  in the second line to regulate the free energy. The cutoff drops out when it comes to comparing the free energies of different solutions.

It is clear from (A.36) that a D6-brane solution of the type (5.4) has always more free energy than a black D6-brane (5.5) or a thermal D6-brane (5.1). Comparing the free energies of the black and thermal D6-brane geometries, we obtain

$$S_{\text{thermal D6}} - S_{\text{black D6-brane}} = \frac{3}{g_s^2} V_9 (u_T - u_{\text{KK}}), \quad (\text{A.38})$$

$$= \frac{3V_9}{16\pi^2 g_s^2 R_{6+1}} (\beta^2 - \beta_c^2), \quad (\text{A.39})$$

where in the second line we have used (5.3) and (5.7), and

$$\beta_c = 2\pi R_c = \frac{4\pi}{3} \sqrt{R_{6+1} u_{\text{KK}}}. \quad (\text{A.40})$$

Thus, there is a phase transition at  $\beta = 2\pi R_c$ , where the thermal D6-brane geometry dominates for  $\beta < 2\pi R_c$  whereas for  $\beta > 2\pi R_c$  the black brane geometry dominates.

**Dq-branes: general analysis.** Having gone through the analysis for the D6-brane, calculating the free energy of non-extremal Dq-branes is straightforward. The relevant parts of the supergravity action (in string frame) are

$$S = -(S_{\text{EH}} + S_{\phi} + S_{\text{RR}} + S_{\text{NS}}), \\ = - \int e^{-2\phi} \sqrt{g} (\mathcal{R} + 4\partial\phi\partial\phi) + \frac{1}{2} \sum_q \int F_{(q+2)} \wedge *F_{(q+2)} + \frac{1}{2} \int e^{-2\phi} H_{(3)} \wedge *H_{(3)}. \quad (\text{A.41})$$

We are interested in backgrounds with  $H_{(3)}$  not turned on, and choose the following ansatz for the metric and the RR  $q$ -form  $C_{q+1}$

$$ds^2 = d\tau^2 + e^{2\lambda(\tau)} dx_{\parallel}^2 + e^{2\tilde{\lambda}(\tau)} dx_c^2 + e^{2\nu(\tau)} d\Omega_k^2, \quad (\text{A.42})$$

$$C_{(q+1)} = A dx^1 \wedge \dots \wedge dx^{q-1} \wedge dx^{q-c} \wedge dx^c, \quad (\text{A.43})$$

where  $k = 8 - q$ , and  $d\Omega_k^2$  is the line element of unit  $k$ -sphere. Again, we have set  $l_s = 1$ . The equation of motion for  $C_{(q+1)}$  has the solution

$$\dot{A} e^{-q\lambda - \tilde{\lambda} + k\nu} = \text{const}. \quad (\text{A.44})$$

The RR action then becomes

$$-S_{\text{RR}} = \int Q^2 e^{q\lambda + \tilde{\lambda} - k\nu} d\tau, \quad (\text{A.45})$$

where, again, we denoted the integration constant by  $Q^2$ . For convenience, we change the variable from  $\tau$  to  $\rho$  defined by  $d\rho = -e^\varphi d\tau$ , where

$$\varphi = 2\phi - q\lambda - \tilde{\lambda} - k\nu. \quad (\text{A.46})$$

Then

$$-S_{\text{RR}} = - \int Q^2 e^{q\lambda + \tilde{\lambda} - k\nu - \varphi} d\rho. \quad (\text{A.47})$$

Following the same argument as we did for  $q = 6$ , it is not hard to see that the action (A.41) takes the form

$$S = \int \left( k(k-1)e^{-2\nu-2\varphi} - q\lambda'^2 - \tilde{\lambda}'^2 - k\nu'^2 + \varphi'^2 - Q^2 e^{q\lambda + \tilde{\lambda} - k\nu} \right) d\rho. \quad (\text{A.48})$$

Having put the action in the above form, the equations of motion are now in order

$$\lambda'' = \frac{Q^2}{2} e^{-2\phi + 2q\lambda + 2\tilde{\lambda}} \quad (\text{A.49})$$

$$\tilde{\lambda}'' = \frac{Q^2}{2} e^{-2\phi + 2q\lambda + 2\tilde{\lambda}} \quad (\text{A.50})$$

$$\nu'' = (k-1)e^{-2\nu-2\varphi} - \frac{Q^2}{2} e^{-2\phi + 2q\lambda + 2\tilde{\lambda}} \quad (\text{A.51})$$

$$\phi'' = \frac{(5-k)Q^2}{2} e^{-2\phi + 2q\lambda + 2\tilde{\lambda}}, \quad (\text{A.52})$$

Define  $\Phi = -2\phi + 2q\lambda + 2\tilde{\lambda}$ , (A.49), then (A.50) and (A.52) result in

$$\Phi'' = 4Q^2 e^\Phi, \quad (\text{A.53})$$

which yields the following solution

$$\Phi = -2 \ln \left( \frac{\sqrt{2}Q}{CC_1} \sinh C_1 \rho \right) - 2 \ln C. \quad (\text{A.54})$$

The last term is there just for convenience. Solving for  $\lambda$ ,  $\tilde{\lambda}$  and  $\phi$  in (A.49), (A.50) and (A.52), we obtain

$$\lambda = -\frac{1}{4} \ln \left( \frac{\sqrt{2}Q}{g_s C_1} \sinh C_1 \rho \right) + C_2^\lambda \rho, \quad (\text{A.55})$$

$$\tilde{\lambda} = -\frac{1}{4} \ln \left( \frac{\sqrt{2}Q}{g_s C_1} \sinh C_1 \rho \right) + C_2^{\tilde{\lambda}} \rho, \quad (\text{A.56})$$

$$\phi = -\frac{5-k}{4} \ln \left( \frac{\sqrt{2}Q}{g_s C_1} \sinh C_1 \rho \right) + C_2^\phi \rho + \ln g_s, \quad (\text{A.57})$$



with  $qC_2^\lambda + C_2^{\bar{\lambda}} - C_2^\phi = 0$ . The constants  $C_1$ ,  $C_2^\lambda$ ,  $C_2^{\bar{\lambda}}$  and  $C_2^\phi$  are to be determined. Define  $\Phi_0 = \Phi + 2 \ln g_s$ , then the equation of motion for  $\nu$  becomes

$$\nu'' = (k-1)e^{\frac{7-q}{4}\Phi_0 - 2C_2^\phi\rho - 4\ln g_s + 2(k-1)\nu} - \frac{1}{2}Q^2e^\Phi. \quad (\text{A.58})$$

If we take  $2(k-1)\nu = \frac{q-3}{4}\Phi_0 + 2C_2^\phi\rho + C_\nu$ , then the above equation is satisfied if

$$C_\nu = \ln \frac{2Q^2g_s^2}{(k-1)^2}. \quad (\text{A.59})$$

Thus, we obtain

$$\nu = -\frac{5-k}{4(k-1)} \ln \left( \frac{\sqrt{2}Q}{g_s C_1} \sinh C_1 \rho \right) + \frac{C_2^\phi \rho}{k-1} + \frac{1}{k-1} \ln \frac{\sqrt{2}Qg_s}{k-1}. \quad (\text{A.60})$$

We now check whether the near horizon geometry of non-extremal Dq-branes satisfies (A.55), (A.56), (A.57) and (A.60). This geometry takes the form

$$ds^2 = f_q^{-1/2} \left( dx_{\parallel}^2 + h dx_c^2 \right) + f_q^{1/2} \left( \frac{1}{h} du^2 + u^2 d\Omega_k^2 \right), \quad (\text{A.61})$$

$$e^{-2\phi} = g_s^{-2} f_q^{(q-3)/2}, \quad (\text{A.62})$$

where  $f_q = \frac{d'_q g_s N_c}{(l_s u)^{7-q}}$ ,  $d'_p = (2\sqrt{\pi})^{5-q} \Gamma(\frac{7-q}{2})$  and  $h = 1 - (u_c/u)^{7-q}$ . The relation between  $u$  and  $\rho$  can be inferred from (A.55) and (A.56)

$$e^{2(\bar{\lambda}-\lambda)} = e^{2\rho(C_2^{\bar{\lambda}}-C_2^\lambda)} = h, \quad (\text{A.63})$$

which gives

$$\rho = \frac{1}{2\Delta C_2} \ln h \quad \Rightarrow \quad d\rho = \frac{(7-q)u_c^{7-q}u^{q-8}}{2\Delta C_2} \frac{1}{h} du, \quad (\text{A.64})$$

where  $\Delta C_2 = C_2^{\bar{\lambda}} - C_2^\lambda$ . Calculating  $e^{2\lambda}$  from (A.55), we have

$$\begin{aligned} e^{2\lambda} &= \frac{e^{2C_2^\lambda \rho}}{\sqrt{\left(\frac{\sqrt{2}Q}{g_s C_1}\right) \sinh C_1 \rho}} \\ &= \sqrt{\frac{\sqrt{2}C_1 g_s}{Q}} \frac{h^{\frac{C_2^\lambda}{\Delta C_2}}}{\sqrt{h^{\frac{C_1}{2\Delta C_2}} - h^{\frac{-C_1}{2\Delta C_2}}}} \\ &= \sqrt{\frac{\sqrt{2}C_1 g_s}{Q}} \frac{h^{\frac{C_2^\lambda}{\Delta C_2} - \frac{C_1}{4\Delta C_2}}}{\sqrt{1 - h^{\frac{-C_1}{\Delta C_2}}}}. \end{aligned} \quad (\text{A.65})$$

The only way to make  $e^{2\lambda}$  in (A.65) to be equal to  $f_q^{1/2}$  is by imposing  $-C_1 = \Delta C_2$  and  $C_1 = 4C_2^\lambda$ , or

$$C_1 = 4C_2^\lambda; \quad C_2^{\bar{\lambda}} = -3C_2^\lambda. \quad (\text{A.66})$$

Thus, we have

$$e^{2\lambda} = \sqrt{\frac{\sqrt{2}C_1 g_s}{Q}} \left(\frac{u}{u_c}\right)^{\frac{7-q}{2}} \equiv f_q^{-1/2} \Rightarrow C_2^\lambda = \frac{Q(u_c l_s)^{7-q}}{4\sqrt{2}g_s^2 N_c d'_q}. \quad (\text{A.67})$$

Also, the dilaton can be matched to (A.62) as long as we take  $C_2^\phi = (5-k)C_2^\lambda$  resulting in

$$e^{2\phi} = e^{2\lambda(5-k)+2\ln g_s} = g_s^2 f_q^{-\frac{q-3}{2}}. \quad (\text{A.68})$$

Furthermore, from (A.60), we have

$$e^{2\nu} = \left(\frac{\sqrt{2}Qg_s}{k-1}\right)^{\frac{2}{k-1}} e^{2\lambda\frac{5-k}{k-1}} \equiv f_q^{1/2} u^2 \Rightarrow N_c = \frac{\sqrt{2}Q l_s^{k-1}}{(k-1)d'_q}. \quad (\text{A.69})$$

The final check is the  $g_{uu}$  component. To do that, we first need to compute  $e^{-2\varphi}$  which gives

$$\begin{aligned} e^{-2\varphi} &= e^{-4\phi+2q\lambda+2\tilde{\lambda}+2k\nu} \\ &= e^{\frac{6k+2}{k-1}\lambda-8C_2^\lambda\rho+\frac{2k}{k-1}\ln\left(\frac{\sqrt{2}Qg_s}{k-1}\right)-4\ln g_s}. \end{aligned} \quad (\text{A.70})$$

Hence

$$\begin{aligned} d\tau^2 &= e^{-2\varphi} d\rho^2 \\ &= \frac{(7-q)^2 u_c^{2(7-q)} u^{2(q-8)}}{64(C_2^\lambda)^2} \frac{1}{h^2} e^{\frac{6k+2}{k-1}\lambda-8C_2^\lambda\rho+\frac{2k}{k-1}\ln\left(\frac{\sqrt{2}Qg_s}{k-1}\right)-4\ln g_s} du^2 \\ &= f_q^{1/2} \frac{1}{h} du^2, \end{aligned} \quad (\text{A.71})$$

where we have used (A.67) and (A.69) to simplify the expression. Therefore, the exact solution we just found indeed corresponds to the near horizon geometry of non-extremal  $N_c$  D $q$ -branes.

With (A.55), (A.56), (A.57) and (A.60) at hand, it is now straightforward to plug them into (A.48) to get the on-shell action. Changing back to the  $u$  coordinate and being careful about the fact that  $d\rho/du$  is negative, we obtain (here prime denotes  $u$  derivative.)

$$\begin{aligned} S &= -V_9 \int_{u_c}^{\infty} \left\{ \left( -q\lambda'^2 - \tilde{\lambda}'^2 - k\nu'^2 + \varphi'^2 \right) \frac{du}{d\rho} + \left( k(k-1)e^{-2\nu-2\varphi} - Q^2 e^{q\lambda+\tilde{\lambda}-k\nu} \right) \frac{d\rho}{du} \right\} du \\ &= \frac{9-q}{g_s^2} V_9 \int_{u_c}^{\Lambda} (7-q) u^{6-q} du \\ &= \frac{9-q}{g_s^2} V_9 \left( \Lambda^{7-q} - u_c^{7-q} \right), \end{aligned} \quad (\text{A.72})$$

where  $\Lambda$  is the cutoff, and  $V_9 = \beta R_c \text{Vol}(S^{8-q}) \text{Vol}(\mathbb{R}^{q-1})$  (in units where string length  $l_s = 1$ ). For  $q \leq 4$ , it is not hard to see from (A.72) that the geometry given in (5.4) for which  $u_c = 0$  has more free energy than the geometries given in (5.1) and (5.5). The difference in free energies of the thermal and black D $q$ -brane geometries is given by

$$S_{\text{thermal}} - S_{\text{black brane}} = \frac{9-q}{g_s^2} V_9 \left( u_T^{7-q} - u_{\text{KK}}^{7-q} \right), \quad (\text{A.73})$$

which using (5.3) and (5.7) can be equivalently expresses as

$$S_{\text{thermal}} - S_{\text{black brane}} = \frac{9-q}{g_s^2} V_9 \left( \frac{4\pi}{7-q} R_{q+1}^{\frac{1}{2}(7-q)} \right)^{2\frac{7-q}{5-q}} \left( \beta^{2\frac{q-7}{5-q}} - \beta_c^{2\frac{q-7}{5-q}} \right). \quad (\text{A.74})$$

Thus, for  $q \leq 4$  there is a phase transition at  $\beta = 2\pi R_c$ . For  $\beta > 2\pi R_c$  the thermal geometry (5.1) dominates whereas for  $\beta < 2\pi R_c$  it is the black brane geometry (5.5) which dominates the Euclidean path integral. The case of D5-branes and any associated phase transition has been discussed in section 5.

## A.2 Non-compact $x^q$

When  $x^q$  is not compact, and  $q \neq 5$ , there are only two geometries with the same asymptotic boundary condition: the thermal geometry (2.7) and the black brane geometry (2.2). The difference in free energies of the two geometries is obtained by first setting  $u_c = 0$  in (A.72) for the thermal and  $u_c = u_T$  for the black brane geometry, then subtracting the results

$$S_{\text{thermal}} - S_{\text{black brane}} = \frac{9-q}{g_s^2} V_9 u_T^{7-q}, \quad (\text{A.75})$$

where  $V_9 = \text{Vol}(S^{8-q})\text{Vol}(\mathbb{R}^q)\text{Vol}(S^1_\beta)$  in units where  $l_s = 1$ . The difference in free energies (2.8) is positive indicating that independent of temperature the black brane geometry is always dominant and determines the vacuum. The case of D5-branes has been discussed in section 2.

## References

- [1] T. Sakai and S. Sugimoto, *Low energy hadron physics in holographic QCD*, *Prog. Theor. Phys.* **113** (2005) 843 [[hep-th/0412141](#)] [[SPIRES](#)].
- [2] J.M. Maldacena, *The large- $N$  limit of superconformal field theories and supergravity*, *Adv. Theor. Math. Phys.* **2** (1998) 231 [*Int. J. Theor. Phys.* **38** (1999) 1113] [[hep-th/9711200](#)] [[SPIRES](#)].
- [3] S.S. Gubser, I.R. Klebanov and A.M. Polyakov, *Gauge theory correlators from non-critical string theory*, *Phys. Lett.* **B 428** (1998) 105 [[hep-th/9802109](#)] [[SPIRES](#)].
- [4] E. Witten, *Anti-de Sitter space and holography*, *Adv. Theor. Math. Phys.* **2** (1998) 253 [[hep-th/9802150](#)] [[SPIRES](#)].
- [5] O. Aharony, S.S. Gubser, J.M. Maldacena, H. Ooguri and Y. Oz, *Large- $N$  field theories, string theory and gravity*, *Phys. Rept.* **323** (2000) 183 [[hep-th/9905111](#)] [[SPIRES](#)].
- [6] E. Witten, *Anti-de Sitter space, thermal phase transition and confinement in gauge theories*, *Adv. Theor. Math. Phys.* **2** (1998) 505 [[hep-th/9803131](#)] [[SPIRES](#)].
- [7] A. Brandhuber, N. Itzhaki, J. Sonnenschein and S. Yankielowicz, *Wilson loops in the large- $N$  limit at finite temperature*, *Phys. Lett.* **B 434** (1998) 36 [[hep-th/9803137](#)] [[SPIRES](#)].
- [8] E. Antonyan, J.A. Harvey, S. Jensen and D. Kutasov, *NJLS and QCD from string theory*, [[hep-th/0604017](#)] [[SPIRES](#)].
- [9] Y. Nambu and G. Jona-Lasinio, *Dynamical model of elementary particles based on an analogy with superconductivity. I*, *Phys. Rev.* **122** (1961) 345 [[SPIRES](#)].

- [10] O. Aharony, J. Sonnenschein and S. Yankielowicz, *A holographic model of deconfinement and chiral symmetry restoration*, *Annals Phys.* **322** (2007) 1420 [[hep-th/0604161](#)] [[SPIRES](#)].
- [11] A. Parnachev and D.A. Sahakyan, *Chiral phase transition from string theory*, *Phys. Rev. Lett.* **97** (2006) 111601 [[hep-th/0604173](#)] [[SPIRES](#)].
- [12] E. Antonyan, J.A. Harvey and D. Kutasov, *Chiral symmetry breaking from intersecting D-branes*, *Nucl. Phys. B* **784** (2007) 1 [[hep-th/0608177](#)] [[SPIRES](#)].
- [13] N. Itzhaki, J.M. Maldacena, J. Sonnenschein and S. Yankielowicz, *Supergravity and the large- $N$  limit of theories with sixteen supercharges*, *Phys. Rev. D* **58** (1998) 046004 [[hep-th/9802042](#)] [[SPIRES](#)].
- [14] O. Aharony, *A brief review of “little string theories”*, *Class. Quant. Grav.* **17** (2000) 929 [[hep-th/9911147](#)] [[SPIRES](#)].
- [15] M. Kruczenski, D. Mateos, R.C. Myers and D.J. Winters, *Towards a holographic dual of large- $N_c$  QCD*, *JHEP* **05** (2004) 041 [[hep-th/0311270](#)] [[SPIRES](#)].
- [16] N. Horigome, M. Nishimura and Y. Tanii, *Chiral symmetry breaking in brane models*, *JHEP* **02** (2008) 003 [[arXiv:0710.4900](#)] [[SPIRES](#)].
- [17] Y.-h. Gao, W.-s. Xu and D.-f. Zeng, *NGN, QCD<sub>2</sub> and chiral phase transition from string theory*, *JHEP* **08** (2006) 018 [[hep-th/0605138](#)] [[SPIRES](#)].
- [18] D.J. Gross and A. Neveu, *Dynamical symmetry breaking in asymptotically free field theories*, *Phys. Rev. D* **10** (1974) 3235 [[SPIRES](#)].
- [19] J.J. Friess, S.S. Gubser, G. Michalogiorgakis and S.S. Pufu, *Stability of strings binding heavy-quark mesons*, *JHEP* **04** (2007) 079 [[hep-th/0609137](#)] [[SPIRES](#)].
- [20] N. Horigome and Y. Tanii, *Holographic chiral phase transition with chemical potential*, *JHEP* **01** (2007) 072 [[hep-th/0608198](#)] [[SPIRES](#)].
- [21] O. Bergman, G. Lifschytz and M. Lippert, *Holographic nuclear physics*, *JHEP* **11** (2007) 056 [[arXiv:0708.0326](#)] [[SPIRES](#)].
- [22] J.L. Davis, M. Gutperle, P. Kraus and I. Sachs, *Stringy NJLS and Gross-Neveu models at finite density and temperature*, *JHEP* **10** (2007) 049 [[arXiv:0708.0589](#)] [[SPIRES](#)].
- [23] M. Rozali, H.-H. Shieh, M. Van Raamsdonk and J. Wu, *Cold nuclear matter in holographic QCD*, *JHEP* **01** (2008) 053 [[arXiv:0708.1322](#)] [[SPIRES](#)].
- [24] O. Bergman, G. Lifschytz and M. Lippert, *Response of holographic QCD to electric and magnetic fields*, *JHEP* **05** (2008) 007 [[arXiv:0802.3720](#)] [[SPIRES](#)].
- [25] C.V. Johnson and A. Kundu, *External fields and chiral symmetry breaking in the Sakai-Sugimoto model*, *JHEP* **12** (2008) 053 [[arXiv:0803.0038](#)] [[SPIRES](#)].
- [26] K.-Y. Kim, S.-J. Sin and I. Zahed, *Dense and hot holographic QCD: finite baryonic  $E$  field*, *JHEP* **07** (2008) 096 [[arXiv:0803.0318](#)] [[SPIRES](#)].
- [27] M.R. Garousi, *D-brane anti-D-brane effective action and brane interaction in open string channel*, *JHEP* **01** (2005) 029 [[hep-th/0411222](#)] [[SPIRES](#)].
- [28] R. Casero, E. Kiritsis and A. Paredes, *Chiral symmetry breaking as open string tachyon condensation*, *Nucl. Phys. B* **787** (2007) 98 [[hep-th/0702155](#)] [[SPIRES](#)].
- [29] O. Bergman, S. Seki and J. Sonnenschein, *Quark mass and condensate in HQCD*, *JHEP* **12** (2007) 037 [[arXiv:0708.2839](#)] [[SPIRES](#)].

- [30] A. Dhar and P. Nag, *Sakai-Sugimoto model, tachyon condensation and chiral symmetry breaking*, *JHEP* **01** (2008) 055 [[arXiv:0708.3233](#)] [[SPIRES](#)].
- [31] M. Edalati, R.G. Leigh and N. Nguyen, work in progress.
- [32] U.H. Danielsson, A. Guijosa and M. Kruczenski, *Brane-antibrane systems at finite temperature and the entropy of black branes*, *JHEP* **09** (2001) 011 [[hep-th/0106201](#)] [[SPIRES](#)].
- [33] K. Hotta, *Brane-antibrane systems at finite temperature and phase transition near the Hagedorn temperature*, *JHEP* **12** (2002) 072 [[hep-th/0212063](#)] [[SPIRES](#)].
- [34] V. Calo and S. Thomas, *Phase transitions in separated  $D_{p-1}$  and anti- $D_{p-1}$  branes at finite temperature*, *JHEP* **06** (2008) 093 [[arXiv:0802.2453](#)] [[SPIRES](#)].
- [35] O. Aharony and D. Kutasov, *Holographic duals of long open strings*, *Phys. Rev. D* **78** (2008) 026005 [[arXiv:0803.3547](#)] [[SPIRES](#)].
- [36] R. McNees, R.C. Myers and A. Sinha, *On quark masses in holographic QCD*, *JHEP* **11** (2008) 056 [[arXiv:0807.5127](#)] [[SPIRES](#)].
- [37] P.C. Argyres, M. Edalati, R.G. Leigh and J.F. Vazquez-Poritz, *Open Wilson lines and chiral condensates in thermal holographic QCD*, *Phys. Rev. D* **79** (2009) 045022 [[arXiv:0811.4617](#)] [[SPIRES](#)].
- [38] K. Hashimoto, T. Hirayama, F.-L. Lin and H.-U. Yee, *Quark mass deformation of holographic massless QCD*, *JHEP* **07** (2008) 089 [[arXiv:0803.4192](#)] [[SPIRES](#)].
- [39] S. Kuperstein and J. Sonnenschein, *Non-critical supergravity ( $d > 1$ ) and holography*, *JHEP* **07** (2004) 049 [[hep-th/0403254](#)] [[SPIRES](#)].